SANDIA REPORT

SAND2005-5873
Unlimited Release
Printed October 2005

Surrogate/Spent Fuel Sabotage Aerosol Ratio Testing: Phase 1 Summary and Results

M.A. Molecke, R.H. Yoshimura, M.G. Vigil, R.R. Dickey, K.B. Sorenson, W. Koch, O. Nolte, G. Pretzsch, F. Lange, B. Autrusson, and F.I. Young

Prepared by Sandia National Laboratories
Albuquerque, New Mexico 87185 and Livermore, California 94550

Sandia is a multiprogram laboratory operated by Sandia Corporation,
a Lockheed Martin Company, for the United States Department of Energy's
National Nuclear Security Administration under Contract DE-AC04-94AL85000.

Issued by Sandia National Laboratories, operated for the United States Department of Energy by Sandia Corporation.

Available to DOE and DOE contractors from
U.S. Department of Energy
Office of Scientific and Technical Information
P.O. Box 62
Oak Ridge, TN 37831

Telephone: (865)576-8401
Facsimile: (865)576-5728
E-Mail: reports@adonis.osti.gov
Online ordering: http://www.osti.gov/bridge

Available to the public from
U.S. Department of Commerce
National Technical Information Service
5285 Port Royal Rd
Springfield, VA 22161

Telephone: (800)553-6847
Facsimile: (703)605-6900
E-Mail: orders@ntis.fedworld.gov
Online order: http://www.ntis.gov/help/ordermethods.asp?loc=7-4-0#online

SAND2005-5873
Unlimited Release
Printed October 2005

Surrogate/Spent Fuel Sabotage Aerosol Ratio Testing: Phase 1 Summary and Results

M.A. Molecke, R.H. Yoshimura, M.G. Vigil, R.R. Dickey, and K.B. Sorenson
Sandia National Laboratories,* Albuquerque, NM 87185-0718, USA

W. Koch & O. Nolte, Fraunhofer Institut für Toxikologie und Experimentelle Medizin, Germany
G. Pretzsch and F. Lange, Gesellschaft für Anlagen- und Reaktorsicherheit (GRS), Germany
B. Autrusson, Institut de Radioprotection et de Surete Nucleaire (IRSN), France
F.I. Young, U.S. Nuclear Regulatory Commission

ABSTRACT

This multinational test program is quantifying the aerosol particulates produced when a high energy density device (HEDD) impacts surrogate material and actual spent fuel test rodlets. The experimental work, performed in four consecutive test phases, has been in progress for several years. The overall program provides needed data that are relevant to some sabotage scenarios in relation to spent fuel transport and storage casks, and associated risk assessments. This program also provides significant political benefits in international cooperation for nuclear security related evaluations. The spent fuel sabotage – aerosol test program is coordinated with the international Working Group for Sabotage Concerns of Transport and Storage Casks (WGSTSC), and supported by both the U.S. Department of Energy and Nuclear Regulatory Commission. This report summarizes the preliminary, Phase 1 work performed in 2001 and 2002 at Sandia National Laboratories and the Fraunhofer Institute, Germany, and documents the experimental results obtained, observations, and preliminary interpretations. Phase 1 testing included: performance quantifications of the HEDD devices; characterization of the HEDD or conical shaped charge (CSC) jet properties with multiple tests; refinement of the aerosol particle collection apparatus being used; and, CSC jet-aerosol tests using leaded glass plates and glass pellets, serving as representative brittle materials. Phase 1 testing was quite important for the design and performance of the following Phase 2 test program and test apparatus.

* Sandia is a multi-program laboratory operated by Sandia Corporation, a Lockheed Martin Company, for the United States Department of Energy under contract DE-AC04-94-AL85000.

ACKNOWLEDGEMENTS

The authors wish to acknowledge and express gratitude to the major contributions and support by multiple people to the initial surrogate/spent fuel sabotage and aerosol measurement test program definition and conduct of the Phase 1 testing. All of the participants of the international Working Group for Sabotage Concerns of Transport and Storage Casks (WGSTSC) are responsible for the early and continuing successes of this program. Most of the same people have also provided major technical inputs to the writing of this report, and the results and interpretations within. For Sandia National Laboratories personnel, we recognize Adam Jimenez, explosives technician, Don Berry, Susan Longley, Paul Helmick, and Rob Naegeli for providing significant technical coordination and support for preliminary feasibility and nuclear facilities related issues, as did John Guth and Jeff Philbin in the past. Bob Luna, a consultant and retired Sandian, provided an excellent link with the preliminary technical definition and history of this test program. Bill Lake, DOE-retired, Ashok Kapoor, DOE Albuquerque National Transportation Program, and Didier Brochard, IRSN, now at Commissariat a l'Energie Atomique, France, also provided significant input and guidance during the initial phase of test program definition. Professor Michael Huerta, University of Texas, El Paso, provided initial modeling calculations on the conical shape charge jet performance.

Of course, we also give special thanks to Nancy Slater Thompson and Ron Cherry, Department of Energy, and Skip Young and Tin Mo, Nuclear Regulatory Commission, for providing recent major programmatic guidance and support for the successful, continuing conduct of this program.

TABLE OF CONTENTS

TABLES

FIGURES

This page is intentionally blank.

Surrogate/Spent Fuel Sabotage Aerosol Ratio Test Program: Phase 1 Summary and Results

1. INTRODUCTION

This report summarizes the preliminary, Phase 1 work performed as part of a multinational test program to quantify respirable and aerosol particle materials produced from the interaction of a high energy density device (HEDD), i.e., a conical shaped charge (CSC), with surrogate and actual spent fuel materials. We have previously documented [Molecke et al., 2004a] an overview and existing results of the ongoing four-phase test program that supports the needs of the International Working Group for Sabotage Concerns of Transport and Storage Casks (WGSTSC). That document [Molecke et al., 2004] provided the overall program test plan, background, objectives, and described the interface between all current participants. All WGSTSC members participating in Phase 1 of the current test program are listed in Table 1. The WGSTSC is coordinating the overall research to better understand the potential impacts from sabotage of nuclear material shipments and storage casks, to better protect people and the environment against radiological hazards arising from such sabotage.

The present document focuses only on the Phase 1 activities of the overall test program. Goals for the Phase 1 testing included: performance quantifications of the HEDD devices; characterization of the HEDD or CSC jet properties with multiple tests; refinement of the aerosol particle collection apparatus being used; and, CSC jet-aerosol tests using leaded glass plates and glass pellets as representative brittle materials. Seven of these CSC-glass tests were performed in 2002. Phase 1 test conduct was completed in 2002. Phase 1 test data and results presented herein, support quantifications of aerosolized materials produced from actual spent fuel and surrogate material test rods, resulting from an impact by a CSC.

The overall spent fuel/surrogate aerosol ratio tests were initially proposed [GRS/SNL, 2000] as a joint project by GRS and Sandia National Laboratories, at a WGSTSC technical meeting in 2000. The participants endorsed the need for the testing program and initiated planning. The Phase 1 tests, as originally defined [GRS/SNL, 2000], as shown in Figure 1, were to include pre-experiments with aerosol collection and classification units performed to:

- Study the energy transfer between projectiles having various speeds (bullet speeds, high-speed gas guns, up to and including a CSC, HEDD jet) and surrogate brittle material specimens with and without cladding.
- Verify the scaling laws for the size distributions.
- Obtain information on the necessary size of the final aerosol test chamber suitable for subsequent Phase 3 and Phase 4 radioactive experiments in a suitable nuclear facility test cell.
- Find out the necessary precautions to be taken for proper CSC blast shielding of the aerosol instrumentation, and …
- Optimize the basis design for the aerosol particle collection apparatus and test chamber.

Preliminary experiments in Phase 1 testing were performed in Fraunhofer Institute für Toxikologie und Experimentelle Medizin (ITEM) facilities in Germany. These experiments, other sup-

porting German basic research on fragmentation of brittle materials, and some analysis of early Phase 2 tests with cerium oxide surrogate targets, are summarized in APPENDIX A. The later Phase 1 experiments relating to CSC aspects were performed at SNL. There is significant testing cooperation between both organizations.

Table 1. Test Phase 1 WGSTSC Participants

International Working Group for Sabotage Concerns of Transport and Storage Casks	
Country:	Organization:
U.S.A.	Sandia National Laboratories, SNL • Dept. 6141, Materials Transportation Testing and Analysis • Dept. 2554, Explosive Technologies Group • Center 6700, Radiation Sciences/Nuclear Facility Operations
U.S.A.	U.S. Department of Energy, DOE • Environmental Management, National Transportation Program (< FY 2003) • Office of Civilian Radioactive Waste Management, OCRWM, RW-30E, Office of National Transportation • National Nuclear Security Agency, NNSA, NA-243, Office of International Safeguards
U.S.A.	U.S. Nuclear Regulatory Commission, NRC • Nuclear Material Safety and Safeguards, NMSS/SFPO (< FY 2003) • Nuclear Security and Incidence Response, NSIR (FY 2003-2004)
Germany	Gesellschaft für Anlangen- und Reaktorsicherheit , GRS Bundesministerium für Umwelt Naturschutz und Reaktorsicherheit, BMU
Germany	Fraunhofer Institut für Toxikologie und Experimentelle Medizin, ITEM (previously: Institut für Toxikologie und Aerosolforschung, ITA)
France	Institut de Radioprotection et de Surete Nucleaire, IRSN (previously, IPSN)
UK	Office for Civil Nuclear Security, OCNS, Department of Trade and Industry

Following the conduct of the Phase 1 tests, the overall surrogate/spent fuel sabotage aerosol test program and original test matrix, shown in Table 2, was expanded [Luna et al., 2002] and then documented in Sandia Technical Report SAND2004-1832 [Molecke et al., 2004a]. Test plan details and initial results and plans for Phase 2 (cerium oxide surrogate), Phase 3 (unirradiated depleted uranium oxide surrogate), and Phase 4 (actual uranium oxide spent fuel test rodlet) testing and results, interpretations, comparisons, etc., are documented separately [Molecke et al., 2003, 2004a, and 2004b].

Table 2. Original Representative Test Matrix [GRS/SNL, 2000]

Phase/ Test	Target Material	Number of Rod Targets	CSC* Used	Jet Tip Speed (10^3 m/s)	Comments/Notes
1 / 1, 2,…	Glass / DUO_2	1, 3 or 5	CSC1	≈ 9	Checkout and shakedown tests
2 / 1	DUO_2	1	CSC1	≈ 9	
2 / 2	DUO_2	1	CSC1	≈ 9	Duplicate for comparison to 2/1
2 / 3	DUO_2	1	CSC2	≈ 9	Same tip speed as CSC1, but with d_i / d_p = <0.2 as goal
2 / 4	DUO_2	5	CSC1	≈ 9	To look at aerosol from collateral effects on adjoining rods
3 / 1	Spent Fuel	1	CSC1	≈ 9	
3 / 2	Spent Fuel	1	CSC1	≈ 9	Duplicate for comparison to Experiment No. 3/1
3 / 3	Spent Fuel	1	CSC2	≈ 9	Analogously to Experiment No. 2 / 3 (If funding is available)

* Conical Shaped Charge - CSC1 is a commercially available CSC used in most Phase 1, and all subsequent Phase 2, 3, and 4 tests. CSC2 is a smaller, research-type CSC with less explosive content and a smaller jet diameter. (Refer to Section 3)

2. BACKGROUND: AEROSOL SCALING LAW

In a meeting at the Fraunhofer Institute (ITEM) in Hannover, Germany, on May 25, 2001, personnel from the NRC, SNL, GRS, and Fraunhofer agreed that the linearity of the aerosol scaling law for brittle materials (including ceramic fuel pellets of uranium oxide, among others) must be confirmed for CSC impact velocities, and that this validation should be conducted prior to initiation of the feasibility study for conduct of explosives and radioactive dispersion experiments at a hot cell facility (the final phases of the test program). Because the validity of the scaling law was untested for impact velocities greater than 1 km/sec (approximately bullet velocities), proposed high velocity CSC tests would subject representative brittle surrogate materials, such as glass pellets, rods, and plates, to impacts from projectiles traveling at velocities very much greater than 1 km/sec.

If the linearity of the aerosol scaling law is shown to hold at CSC (HEDD) jet impact velocities, ~ 8 km/sec, then the test hardware to measure the particles released from surrogate and real spent fuel materials at CSC velocities can be simplified. Specifically, the centrifugal classifier, vertical elutriator apparatus used by Fraunhofer ITEM to measure particles from 10 to 100 μm aerodynamic diameter (AED) could be replaced or modified for the Phase 4 tests that use highly radioactive spent fuel. This test sampling modification would greatly simplify the measurement process for the Phase 3 surrogate DUO_2 and Phase 4 spent fuel tests that require total particulate containment in a nuclear facility. The measurement of aerosols up to 10 μm AED could be performed with cascade impactor particle collection devices and the collection of aerosol particles up to 100 μm AED could be performed using a velocity and gravity separation technique, i.e., by vertical elutriation.

Earlier tests conducted at Fraunhofer Institut with a gas gun used rigid projectiles, and a scaling law for aerosols from brittle materials was developed for projectile impacts up to ½ km/sec. Refer to APPENDIX A for further detail. A graph developed from the gas gun impact tests that demonstrate the linearity of two scaling law parameters, specific energy input versus cumulative particle size for glass plate tests, is shown in Figure 1.

In the initially proposed testing program [GRS/SNL, 2000], the Fraunhofer Institute, with funding from the German BMU through GRS, would provide the aerosol test chamber and will support the performance of these scaling law validation tests. The vertical elutriation test chamber was fabricated by Fraunhofer and sent to Sandia in 2001. SNL would conduct high velocity projectile tests (initially proposed as two calibration tests and four measurement tests) and use the Fraunhofer aerosol collection chamber. Specimens include glass plates and pellets or short glass rods, to validate brittle material aerosol scaling laws for particles up to 100 microns in diameter at impact velocities much greater than 1 km/sec. Other targets (e.g., powders, glass rods in tubes simulating fuel rods), duplicate tests, or tests at lower velocities will be performed based upon available funding.

SNL will furnish the CSCs, the facility where the experiments will be performed, and conduct the explosive tests. The performance of aerosol measurements, including setup and analyses, was conducted by SNL, with significant assistance by Fraunhofer. Initial plans to use the Lovelace Respiratory Research Institute, in New Mexico, for aerosol support with funding through a contract with Sandia, were not realized.

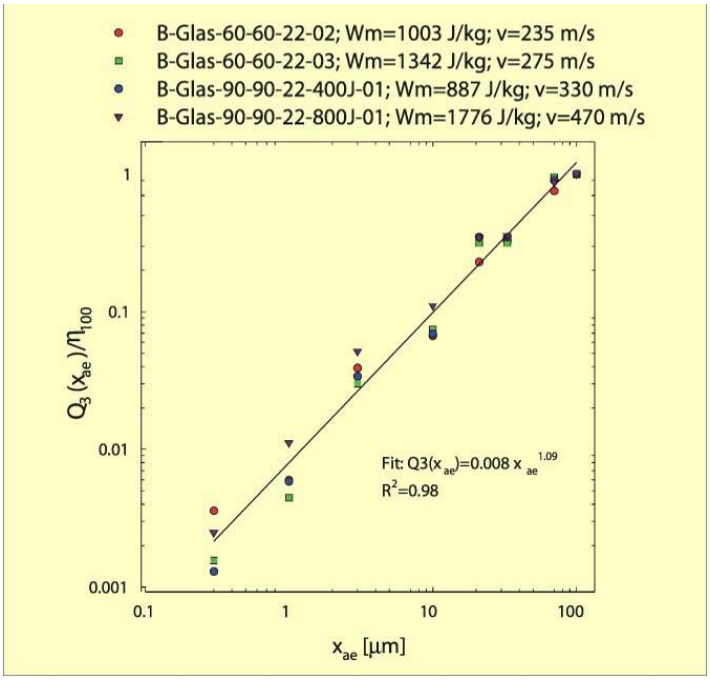

Figure 1. Cumulative Particle Size Distribution vs. AED (µm), Glass Slabs

3. CONICAL SHAPE CHARGE TESTING

In FY2001, a 19 mm (¾-inch) diameter, research-type conical shaped charge ("CSC2" in Table 2) was selected for the aerosol scaling law verification tests because of its small size and low explosive weight. It was presumed that the resultant jet from CSC2 would particulate a single surrogate or spent fuel pellet, thereby simplifying aerosol particle analyses and interpretations. In October 2001, several calibration tests were conducted at Sandia's Explosive Component Facility (ECF) with the research CSC2. These results indicated that CSC2 would not provide a jet of sufficient diameter and length; also, jet parameter results were non-reproducible. Thus, CSC2 would not adequately function as intended for the future aerosol tests. The failure of the research CSC2 required a search for a new, larger CSC ("CSC1" in Table 2). The search yielded a commercially-available, nominal xx gram explosive CSC. Twenty units were procured and delivered in January 2002 for further characterization and jet qualifications.

SNL Explosives Component Group, Department 2554 personnel performed eight tests of the candidate, larger-diameter CSC (CSC1) to obtain jet velocity, diameter, stand off, and to verify the performance of the slug-stopping hardware. The tests were conducted in a large explosive test cell at the SNL Explosives Component Facility (ECF). The candidate CSC performed satisfactorily, and additional units were ordered for the aerosol scaling law verification tests. Figure 2 shows this CSC, as used for all subsequent explosive-aerosol tests; the internal copper cone is visible at right. The CSC jet is formed when the explosive material in the CSC detonates, explosively compressing the copper cone, forming a thin, ~ 1 mm-thick jet that can be visualized as intermediate between a copper plasma or a molten copper wire. A step gage is shown to the right of the conical shaped charge in Figure 2.

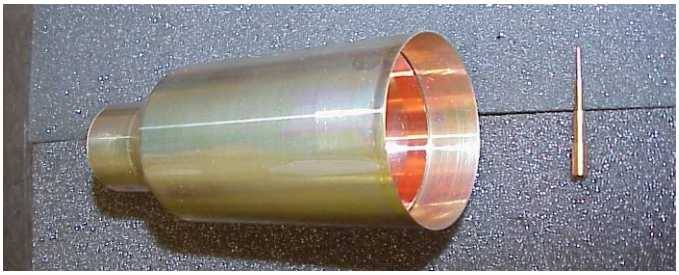

Figure 2. Conical Shaped Charge, CSC1

During the first part of the FY 2002, testing efforts at SNL were focused on CSC1 characterizations and preparations for conducting the scaling law verification tests using a large GRS and Fraunhofer-designed, vertical elutriation aerosol collection chamber. This vertical elutriation chamber was used in multiple laboratory tests at ITEM; it was shipped to SNL on loan, for further CSC and aerosol testing.

As part of the preparations for the scaling law validation tests, SNL constructed a simulated test chamber, based on the Fraunhofer chamber, for proof testing, i.e., to determine if this large aerosol chamber could withstand blast pressures generated by a CSC. Figure 3 shows the simulated (SNL) chamber prior to proof testing. The CSC is mounted (not visible) on the right side of the chamber; the CSC jet travels from right-to-left, through the box, and is stopped in the large steel plates positioned to the left of the chamber. The simulated (SNL) chamber could not withstand the blast pressures and failed; there were significant cracks in the front Lexan face plate, Figure

4, and failed screw attachments plus split seams along the box corners, Figure 5. Subsequently, the Fraunhofer vertical elutriator test chamber was not used at SNL; it was returned, undamaged, to Fraunhofer.

Figure 3. Simulated Vertical Elutriator Chamber, prior to CSC proof testing

Figure 4. Simulated Vertical Elutriator Chamber, cracked Lexan Plate

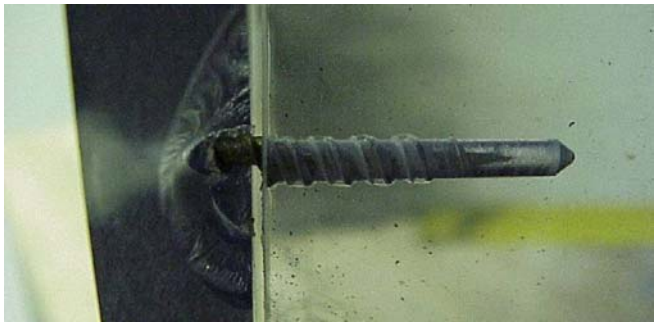

Figure 5. Simulated Vertical Elutriator Chamber, failed corner screw attachment

A new aerosol collection chamber/box was fabricated from welded plates of aluminum 1.2 cm-thick, with two 1.6 cm-thick Lexan viewing windows placed in the sides of the box. This non-ventilated, aerosol collection chamber box, 30 x 40 x 50 cm in size (width x length x height), 12 x 16 x 20 inch, was used for all subsequent Phase 1 tests, and early Phase 2 tests 2/0, 2/1A, 2/1B, 2/2A, and 2/2B [Molecke et al., 2004a]. These windows could be opened (un-bolted) for pretest target insertion and post-test target and residual particulate sampling. There are also small, open holes, about 1.9 cm-diameter, in both the front and back walls, to allow the CSC jet to enter and exit (after penetrating through the surrogate pellet rod target), before being stopped in the adjacent CSC jet stop block. Therefore, this test chamber box does not provide total containment of all particles generated during CSC testing; some particles exit through these holes. This box would be tested with and without Styrofoam (Styropor) sheets on the inside walls to determine if a substantial fraction of fine particles are deposited on the wall of the chamber and to estimate trajectories of the fine particles produced by the CSC impact.

Figure 6 shows the aluminum square box aerosol chamber, with a surrounding measurement grid, and rest of the test setup for calibrating the CSC, in one of the explosive test chambers at the ECF. Three vertically aligned flash X-ray heads are visible in the foreground. The CSC and its holder are mounted to the right of the vertical steel blast shield, the CSC jet stopping plates are on the left side.

Figure 6. Phase 1 Test Setup and Aerosol Collection Box

Four calibration tests (without any target materials in front of the jet) were performed to obtain the characteristics of the jet. The jet tip velocities ranged from 8.0 to 8.5 km/sec and the jet diameter was 1.27 mm (0.05 inch). An example flash X-ray radiograph is shown in Figure 7. This radiograph shows three X-rays shot from different angles of the CSC jet in flight, traveling from right to left. The numbers next to the jet are X-ray reference times, in microseconds. With the distance measurements and time, the velocity of the jet can be calculated. The step gage (calibrated in one-inch steps) shown in the picture provides a reference mark for dimensional measurements. SCAP (shape charge analysis program) modeling was also used to estimate the jet ve-

locity. The jet tip has a fully-formed head (appears as a reverse arrowhead in the radiograph). Jet tip speed and diameter were calculated from measurements of the radiograph. There is some curving of the jet when compared to the grid lines that was later determined to be detrimental to the performance of the slug-stopping hardware. Figure 8 shows another X-ray image taken at a slightly earlier time, in a separate test, showing a solid, continuous jet. At later times in Figure 7, the jet has started to particulate beyond its effective stand off distance, it is no longer continuous.

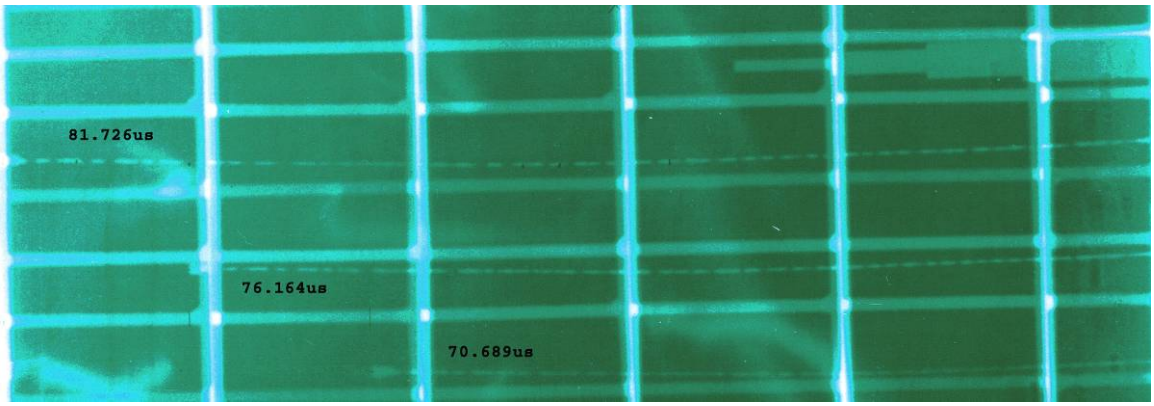

Figure 7. Three superimposed Flash X-rays of the CSC jet during calibration test

Figure 8. Flash X-ray of the CSC jet at 55.6 μsec

In addition to the three diagnostic flash X-rays, a high-speed Imacon camera (~ 30,000 frames/ sec, visible light spectrum) was also used to record the jet in flight. The Imacon camera images indicated that a large amount of explosive detonation combustion by-products would be introduced into the chamber from the CSC. Figure 9 shows the Imacon images from CSC calibration test 3, about 65 μsec after detonation; the jet is traveling to the left in this figure. Part of the combustion products, primarily carbon-based soot particles, appeared luminescent; no real detail could be observed, only light reflected off of dispersed explosive dust and particles.

Further details on the CSC (CSC1) and information on the jet characteristics are found in APPENDIX B [Vigil, 2003a]. In order to resolve potential safety concerns about post-detonation safety concerns relating to the detonation by-products in SNL nuclear facilities and elsewhere, Vigil documented [Vigil, 2003b] the composition of the CSC post-detonation reactant products, the potential for post-test, unsafe conditions, due to the initiation to detonation of un-detonated explosive material, and further information for technical justification and references. This information is contained in APPENDIX C.

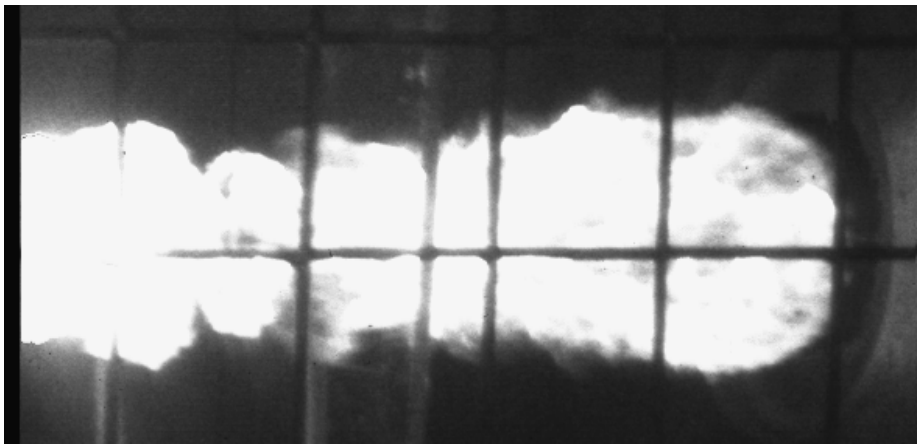

Figure 9. Imacon Camera Image of CSC Detonation Products

German test participants originally requested that the CSC "slug" be stopped and not permitted to strike the glass test specimens, so that a specific energy per unit mass calculation could be made. The slug is a "carrot" shaped mass that is the residue of the post-detonation, CSC copper cone; the slug follows, and travels significantly slower than the jet. The slug is much larger than the tip (front) of the jet and could cause a greater amount of aerosol to be produced. This complexity to determine the specific energy per unit mass parameter is not desirable. Therefore, methods were investigated to stop the slug and prevent it from impacting the test specimen.

Four tests were conducted to evaluate the performance of the slug-stopping hardware. An alloy of tungsten was selected as the stopping block material because of its high density and because it was less expensive than tantalum.

1. The first of these tests used a 50.8-mm (2-inch)-thick tungsten cylinder with a 2.54-mm (0.10-inch)-diameter hole for the jet to pass through. Results from this test indicated that the hole was too small for the jet.

2. The second test used a 31.8-mm (1¼-inch)-thick tungsten cylinder with a 5-mm (0.20-inch)-diameter hole. The slug passed completely through the tungsten slug-stopping block.

3. The third test used a 50.8 mm thick tungsten cylinder with a 5 mm diameter hole.

4. The fourth test used the same configuration as the third, but with less stand-off distance for the CSC.

These tests demonstrated that the slug could be stopped with the appropriate pass-through hole and tungsten block thickness, while the jet passes through. Refer to Figure 10.

Both the flash X-rays and Imacon camera were used to record the jet in flight for CSC slug-stopping test 3. Figure 11 shows three superimposed x-rays taken of the jet after passing through the tungsten cylinder. The numbers shown next to the jet are reference times in µsec of when the X-rays were taken. While the goal of stopping the slug was achieved, the radiograph, Figure 11, shows that the tip of the jet was fragmented. Thus, it would be difficult to obtain an accurate specific energy per unit mass for the tip of the jet impacting the test specimen, and the energy of the jet would be dissipated over a larger area of the target.

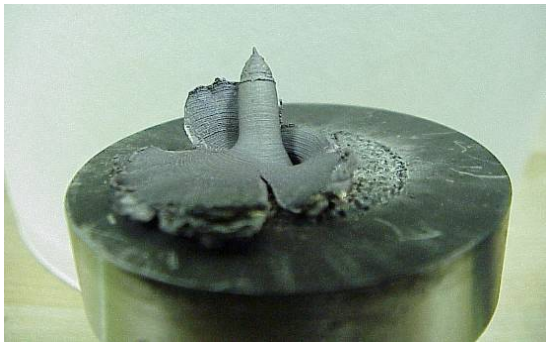

Figure 10. CSC Slug stopped by Tungsten Block, with Hole

Figure 12 shows the Imacon camera image of explosive combustion products passing through the tungsten cylinder about 65 µsec after detonation, well before the slug hits the stopping block. The jet is traveling to the left in both Figures 11 and 12. The small hole in the tungsten slug-stopping hardware did not prevent, but reduced the amount of, combustion products that flowed into the aerosol collection chamber. It is not possible to claim, nor guarantee, that the stopped slug effectively seals the hole in the stopping block, nor prevents combustion products from passing through. The presence of combustion products and particles from the copper CSC jet and tungsten slug-stopping hardware in the aerosol collection chamber could make the initially planned gravimetric measurement (only) technique for determining the amount of aerosols less accurate. This observation was conveyed to the Fraunhofer Institute for consideration. As a result, other measurement techniques, such as using tracer elements in the glass test specimen, were investigated. In Phase 2 of the overall test program, chemical dissolution of the collected aerosol particles, with analysis by inductively coupled mass spectrometry (ICP/MS) was added, in addition to gravimetric analysis [Molecke, 2004a].

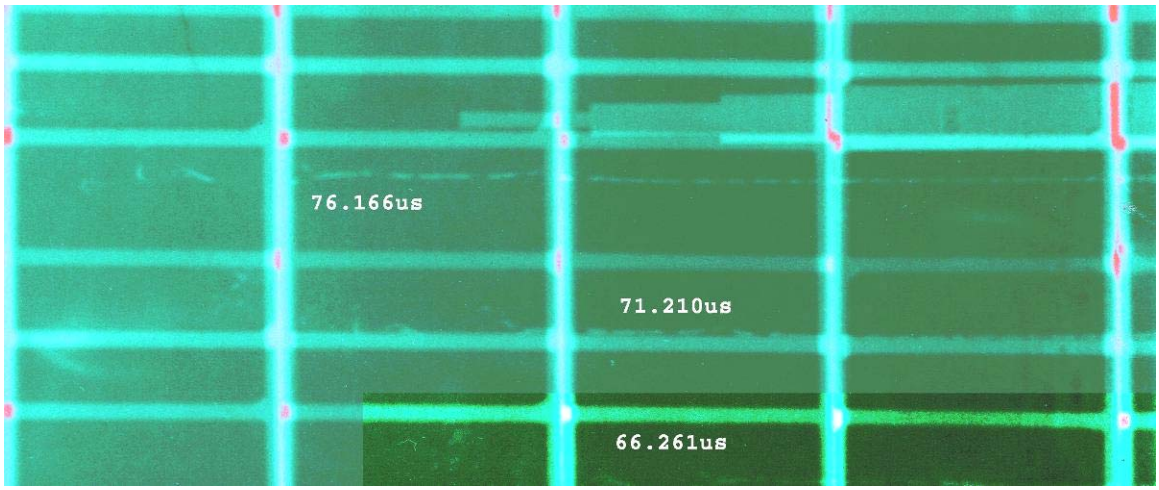

Figure 11. Three superimposed X-rays of CSC jet passing though the tungsten cylinder in slug-stopping test 3.

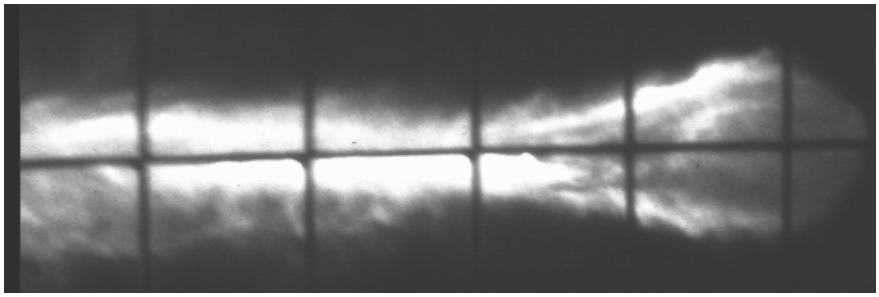

Figure 12. Imacon camera image of combustion products passing through the tungsten cylinder, CSC slug-stopping test 3

SNL staff reviewed the data from this series of tests to determine the best way to proceed with the following aerosol scaling law verification tests, to incorporate known difficulties and concerns. The review yielded two potential options for executing the following Phase 1 glass plate experiments. The options are based on the following, summarized information:

- The CSC (CSC1) is a good HEDD component with reliable tip velocity (about 8.5 km/sec) and a working stand off of about 203 to 229 mm (8 to 9 inches). The observed jet trajectory has deviations from the central axis of the jet equal to about three to four times its diameter. This small deviation is more than adequate for hitting planned targets for the aerosol tests, but has implications for stopping the slug.
- Catching the slug with a tungsten alloy cylinder drilled to pass the jet and retain the slug requires a hole that is too small to allow the jet to pass unimpeded. As a result, the jet is diffused and poorly defined with regard to speed and dimension.
- The jet interaction with the edges of the hole in the tungsten alloy cylinder causes spallation of tungsten material into the test aerosol collection chamber; refer to Figure 13. Any other material in the path of the jet will probably release particulated material into the aerosol chamber.

Figure 13. CSC Jet Passed Through Solid Tungsten Block, with Spallation

The advantages and disadvantages of the two options are summarized below. There are technical and economic considerations; however, the technical considerations were given greater weight.

Option 1 – Perform the Phase 1 glass plate testing without a slug catcher.

Advantages	Disadvantages
It is simplest.	The slug will follow the jet and *perhaps* produce some additional aerosol. The specific energy per unit mass calculation is made more complex.
It is inexpensive.	Combustion products will enter after the jet and slug and may affect measurements; but if glass or surrogate is doped with a tracer element, that might not be a major disadvantage. The combustion products may rule out measurements of aerosol collected by gravimetric techniques.
The aerosol scaling law verification tests can be conducted as soon as arrangements are made with Fraunhofer.	

Option 2 – Introduce a new slug-catcher design that is just a solid cylinder of material (a tungsten alloy, or other material). The jet would make its own hole in the catcher and the slug would be caught.

Advantages	Disadvantages
No slug to complicate the source of aerosol.	Time and expense. A few experiments and analyses would need to be done to achieve the right material and thickness to catch the slug without reducing the tip speed in the test area below 5 mm/μsec. A few additional experiments would be required to re-characterize the jet after passing through the slug catcher.
The small hole would release fewer products of combustion to the aerosol collection chamber.	Potential for spallation aerosols from the catcher would complicate the analysis. Refer to Figure 12.

On a scientific basis, Option 2 initially seemed desirable, but would result in greater test costs than originally planned, and could produce a degraded jet. Option 1 is the expedient solution and allowed the experiments to proceed. However, some calculations would be necessary to raise confidence that the effect of slug passage through the test specimen would not produce a significant amount of additional aerosols. Option 2 might be less costly if there is some quantitative data on a material and a configuration that is certain to meet the jet velocity threshold and catch the jet.

SNL performed several tests for Option 2 to determine if the slug can be stopped using a solid cylinder of tungsten alloy and if the jet tip is sufficiently defined for the aerosol data reduction. The results indicated that the slug could not be easily stopped with the tungsten cylinder. All further testing was performed using Option 1, with no slug-stopping apparatus.

4. PHASE 1 TESTING, GLASS TARGETS

Objectives for this portion of the test program involve answering the following questions, and measuring performance parameters. The verification of the aerosol scaling laws is still needed to determine if simplification of the aerosol collection equipment could be accomplished.

- How do the leaded glass plate targets disintegrate with CSC jet impact? We need to obtain first results on particle size distribution, to test for power law behavior and exponent.
- What is the typical trajectory of the aerosol and fine particles generated?
- Does a substantial fraction of fine particles deposit on the walls of the chamber? What is the fraction of explosive combustion fumes or soot?
- What is the influence of the aerosol collection chamber walls on fragmentation is there significant secondary particle fragmentation due to wall impact?
- What is the CSC jet impact response of a Zircaloy tube filled with glass pellets, representative of a surrogate nuclear fuel rod?

The new aluminum box aerosol collection chamber and test setup, shown in Figures 6 and 14, was used to address these questions. There is no slug-stopping block. An Imacon high-speed camera and flash X-ray tubes were used to record the particle formation process of the glass target-CSC jet impact. The aerosol chamber box was tested both with and without Styrofoam sheets on the inside walls. The Styrofoam was added to determine if a substantial fraction of fine particles are deposited on the wall of the chamber, to prevent secondary fragmentation from particle-wall collisions, and to evaluate the trajectories of the fine particles produced by the CSC impact.

The aerosol collection equipment incorporated two Respicon^{TM} virtual particle impactors. These Respicon particle samplers were originally designed by, and recommended for use by Koch [Koch, et al., 1999], and were loaned to SNL by Fraunhofer. They were commercially manufactured by TSI Incorporated, Shoreview, MN. Each Respicon has three aerosol particle size collector stages: (1) the top stage collects the *respirable* particle fraction of ~ 0 to 4 μm AED; (2) the middle stage collects the *respirable/thoracic* sub-fraction of ~ 4 to 10 μm AED; and, (3) the bottom stage collects the *inhalable* aerosol fraction of ~ 10 to about 100 μm AED. These Respicon particle samplers require the use of a vacuum pump equipped with a throttle valve, to sample at about 3 L/min. A schematic of the aerosol chamber and particle sampling system is shown in Figure 13, illustrating the (open, pretest) interior of the aerosol collection box covered with Styrofoam. The external measurement grid references are shown on the opposite viewing window. Each leaded glass plate target was held in place by a bent rod fixture provided by Fraunhofer. These leaded glass plates had 65 wt.% lead oxide, PbO_2, a lead fraction of 56.3%, and a density of 6.2 g/cm^3. Glass plate specifications are listed in Table 3.

The Phase 1 leaded glass plate test matrix, Table 3, included four tests that were conducted at SNL in June 2002. Gunter Pretzsch, GRS, and Oliver Nolte, Fraunhofer ITEM, participated in these aerosol tests. Glass particles collected in the Respicon impactors and residual particles collected in the aerosol chamber box were shipped to Fraunhofer ITEM for post-test aerosol analyses. Test results are summarized in Section 5, and were provided by Wolfgang Koch, Fraunhofer ITEM [Koch et al., 2002].

Table 3. Phase 1 Glass Plate-CSC Test Matrix

Test Number	Glass Target	Styrofoam Sheet	Sampling Time
1/1	Plate, 50x50x5 mm, 78.5 g	yes	1 minute
1/2	Plate, 50x50x5 mm, 79.2 g	yes	3 minute
1/3	Plate, 20x20x5 mm, 12.3 g	no	6 minute
1/4	Plate, 50x50x5 mm, 79.6 g	no	1 minute

Imacon camera images of test 2, Figure 15, show the CSC jet (traveling left-to-right) impacting the leaded glass plate at a velocity of 8 km/sec. Super-imposed flash X-ray images of the CSC jet striking the leaded glass plate are shown in Figure 16; the CSC jet, approaching from the left at three separate times, is shown once at impact (98.3 µsec, bottom of Figure 15) and twice after the jet has passed through the plate (101.2 and 104.4 µsec). The glass particle debris generated travels in the same direction as the jet, away from jet impact.

Figure 14. Phase 1 Glass Plate Aerosol Test Chamber and Particle Collectors

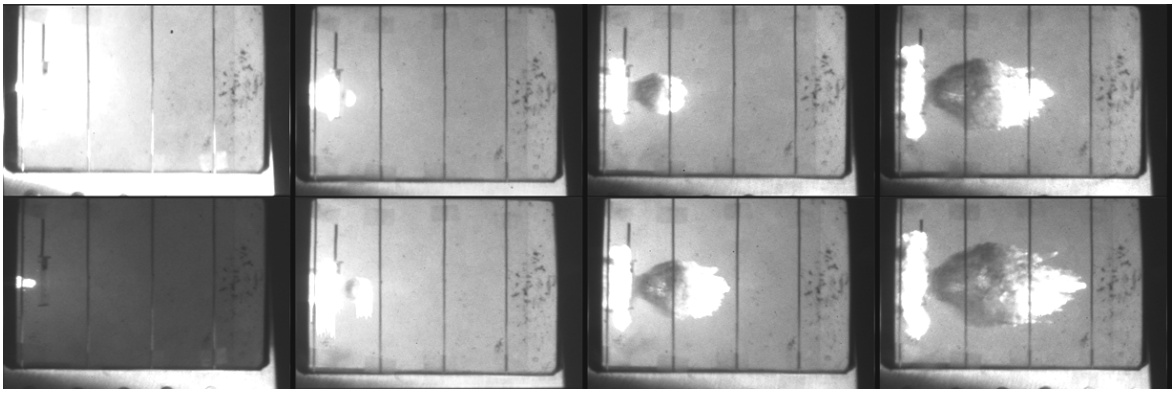

Figure 15. Imacon Camera Images, CSC-Glass Plate Test 2

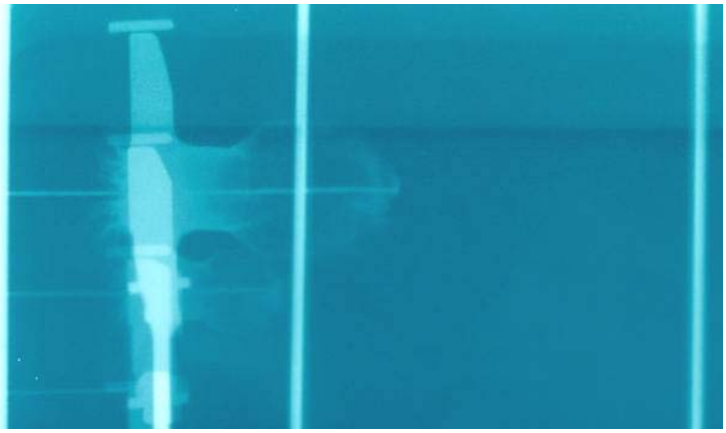

Figure 16. Super-imposed Flash X-ray images of CSC Jet-Glass Plate Impact

The Styrofoam sheets within the aerosol collection box suffered significant damage from the jet and fragments generated within, as shown in the two photographs in Figure 17. Thermal damage resulted in significant soot formation, and mechanical damage was extensive. The use of Styrofoam sheets was discontinued.

Figure 17. Styrofoam Sheet Damage following Explosive-Aerosol Glass Plate Test

Three additional Phase 1 tests were also performed to obtain the response of a Zircaloy tube filled with glass pellets impacted by a CSC jet. The test provided an estimate of how much of the Zircaloy tube would be destroyed by the jet; no aerosol particle collectors were used for these tests. Figure 18 shows the tube and three glass pellets prior to testing. The insert in Figure 18 shows the post-test remains of the Zircaloy tube. Figure 19 shows three X-ray images of the CSC jet (from right-to-left) passing through the Zircaloy tube and glass pellets at several times, with produced particles clearly evident. The damaged area of the tube is much larger than the jet size; no large glass pellet fragments were found, only particles. Figure 19 shows the CSC jet penetrating the glass pellet target at three times, with particle formation. Figure 20 shows the

same test at later times, with the residual CSC slug before and after target impact; the slug does not always travel linearly.

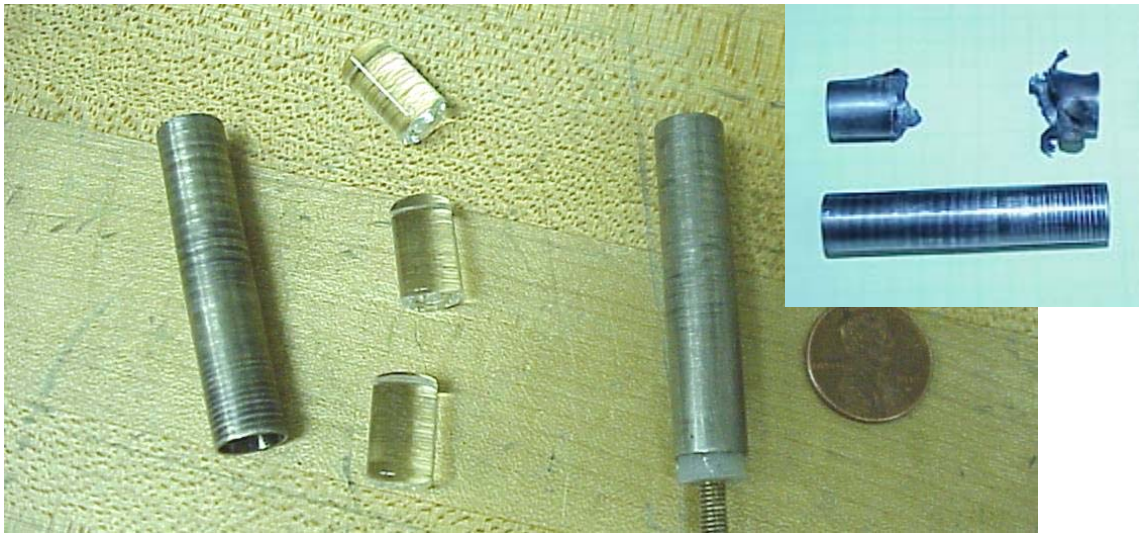

Figure 18. Phase 1 Glass Pellet Zircaloy tube target, pre- and post-test

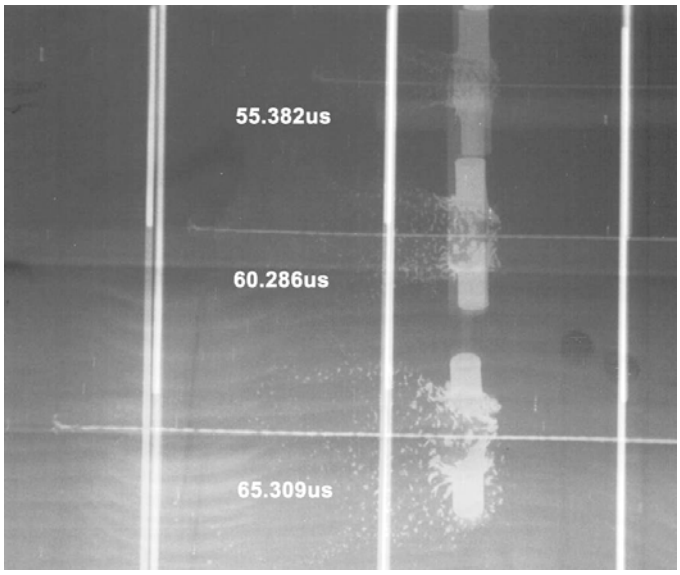

Figure 19. X-ray images of Phase 1 Test Jet, Glass Pellet and Zircaloy Tube

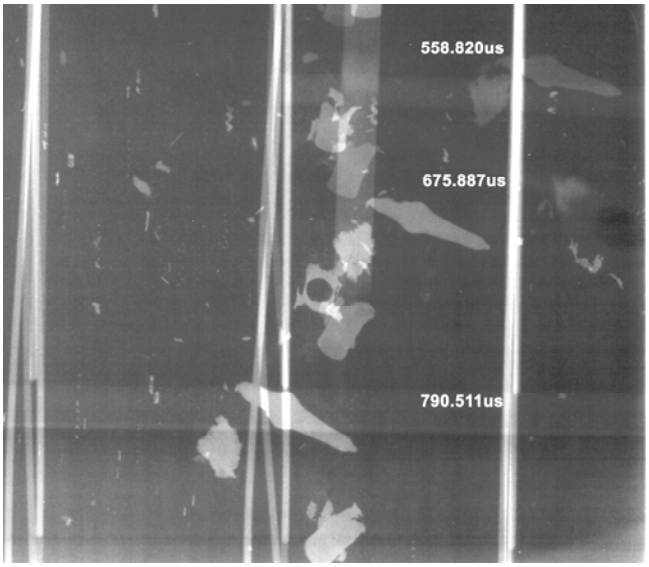

Figure 20. X-ray images of Phase 1 Test Slug, Glass Pellet and Zircaloy Tube

These tests with glass pellet-Zircaloy tube targets were the end of the Phase 1 test program.

5. PHASE 1 TESTING RESULTS

Particle results and observations for the four Phase 1 glass plate – CSC impact tests [Koch et al., 2002] are summarized in this section.

Aerosol particles produced were collected and sampled with two Respicon particle impactors. The first two stages of the Respicons sampled respirable and respirable/thoracic sized particles, in the 0 to ~ 5 µm AED and ~5 to ~ 10 µm AED ranges. The third Respicon stage sampled aerosol particles in the ~ 10 to 100 µm AED range. Respicon samples were used to calculate the respirable glass release fraction (< 10 µm AED) from concentrations. The residual particles within the aerosol collection chamber were collected and removed for mechanical sieve fragment analyses. Laser diffraction analysis was used for the smallest sized residual particles; refer to Figure 21. Chemical analysis of the lead in the leaded glass plate particles was used. In addition, SEM (scanning electron microscope) pictures were obtained for individual particles. Most of the material collected from the aerosol box chamber originates from the glass plates. There was a significant soot contribution only in the small size fractions; this contribution is expected to increase with decreasing particle size.

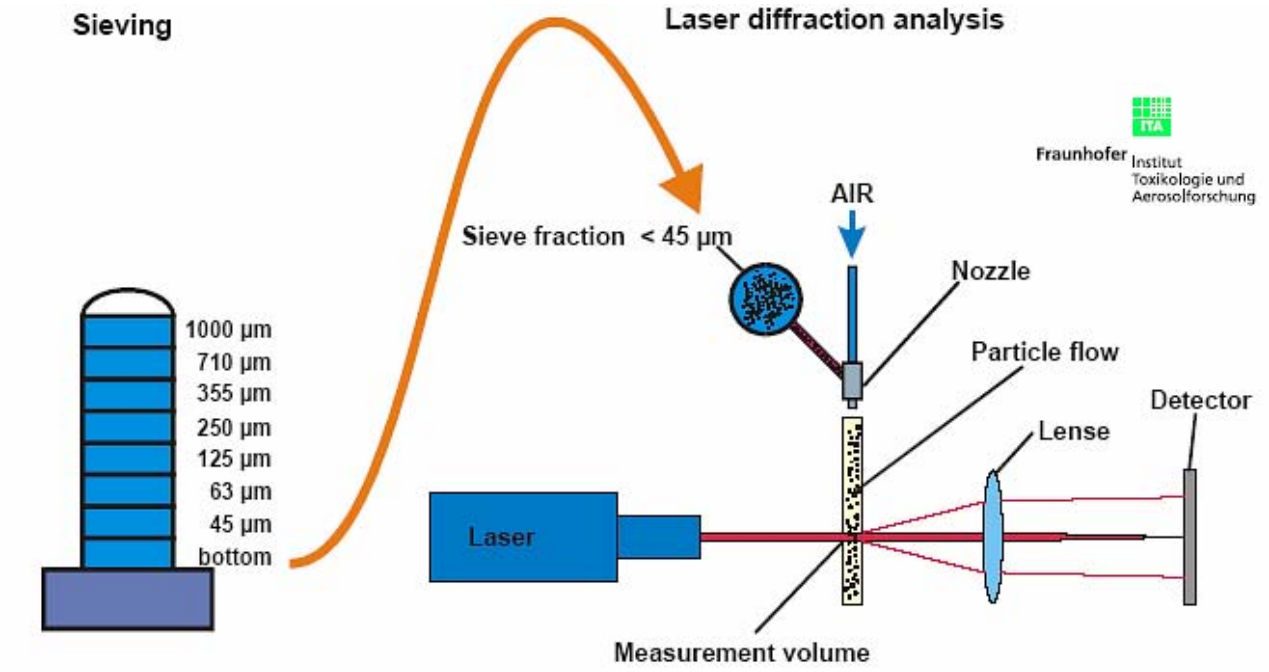

Figure 21. Classification of Recovered Material According to Geometric Diameter

Figures 22 and 23 show the released particle mass of target material in the size range of 0 to < 5 µm AED and 0 to < 10 µm AED, respectively, for all four Phase 1 glass plate tests, based on Respicon concentration measurements and chemical analysis of the lead content. The calculated release fraction for < 5 and < 10 µm AED sized particles is shown in Figure 24. Apparently, there is a significantly lower measured release fraction when the aerosol chamber walls are covered with Styrofoam sheets (tests 1 and 2) than without them (tests 3 and 4). The possible reasons for the lower measure release when the walls are covered with Styrofoam are:

1. Less fine particles are formed, e.g., secondary fragmentation from hard wall contact is lessened.

2. The Respicon sampling inlets may be shadowed by the Styrofoam detachment from the walls due to the explosive detonation; refer to Figure 16.

3. Possibly, even fine particles have a high velocity and are collected or trapped by the Styrofoam, yielding a lower recovery rate.

The target particulate fragments were found predominantly in the Styrofoam covering the bottom and rear wall of the aerosol chamber.

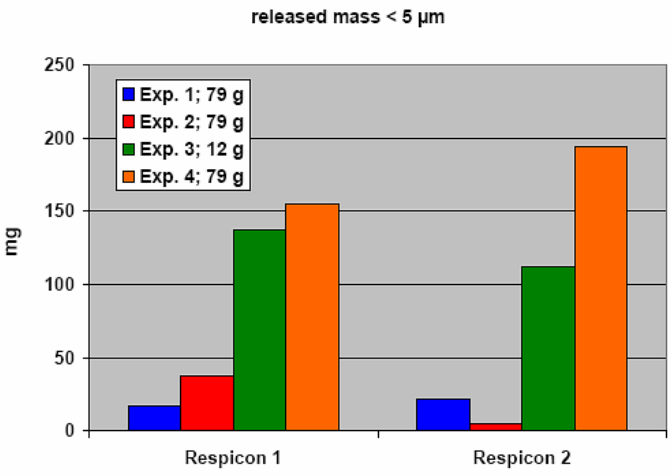

Figure 22. Glass Plate - Respicon Measurements, < 5 µm AED

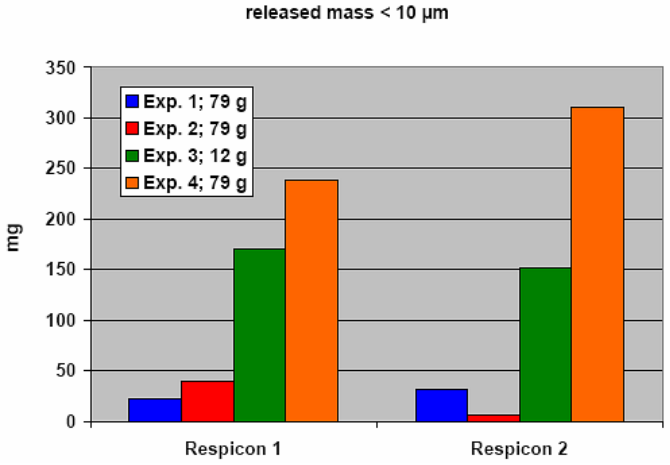

Figure 23. Glass Plate - Respicon Measurements, < 10 µm AED

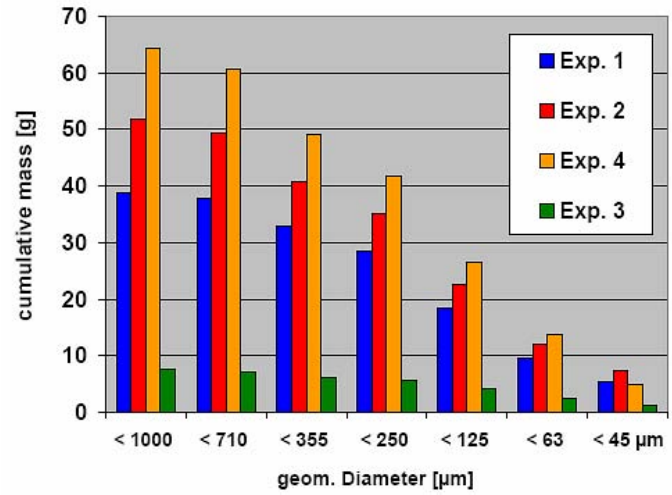

Figure 24. Glass Plate Fragment Sieve Analysis, Cumulative Mass

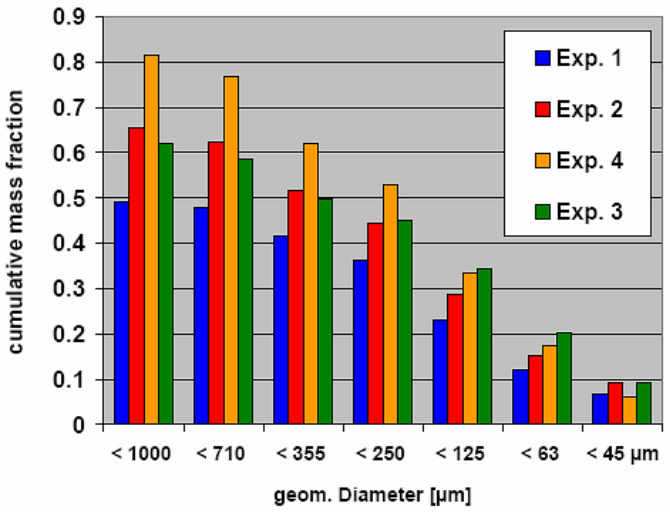

Figure 25. Glass Plate Fragment Sieve Analysis, Cumulative Mass Fraction

Fraunhofer Institut Toxikologie und Aerosolforschung

Results for mechanical sieve analysis of the residual fragments collected in the aerosol box are shown in Figure 24 and 25, respectively, for cumulative mass (in grams) or cumulative mass fraction vs. geometrical particle diameter (in µm). The measured sieve results indicate a relatively small difference between Styrofoam covered (test 1 and 2) and bare chamber walls (tests 3 and 4), particularly in the size range smaller than 45 µm geometric (equivalent to 112 µm AED).

There is a nearly linear increase of cumulative mass with particle size. All four of the Phase 1 glass plate experiments give similar results with respect to the size distribution of the "large" fragments. There is no significant difference between experiments with Styrofoam covered and bare chamber walls in the relevant size fraction below 45 µm geometric.

Laser diffraction spectroscopy (LDS), scanning electron microscopy (SEM), and energy dispersive X-ray spectroscopy (EDX) were used to evaluate sieved particles smaller than 45 µm geometric 4. Both irregular fragments and rounded particles of glass were observed with SEM; the rounded particles indicate that some melting of the glass particles occurred during CSC jet impact. High resolution SEM of the glass particles shows that the particles are covered with a layer of submicron particles, presumably soot from the CSC detonation. The EDX provided analysis of silicon and lead from the leaded glass plate particles, plus copper content from the CSC jet.

Particle size evaluations from the Respicon impactors, sieve measurements and LDS for all four tests are shown in Figure 26. The Respicon and LDS measurements agree surprisingly well. (Respicon measurements from test 1 and 2 were disregarded due to losses of particles in the Styrofoam layer in test 1 and 2. All four tests appear quite reproducible, in view of the large fragments formed. There is relatively large scatter in the small particle size data, < 10 µm AED; test 3 (with the smaller sized glass plate) results are significantly different, greater than respirable results from tests 1, 2, and 4

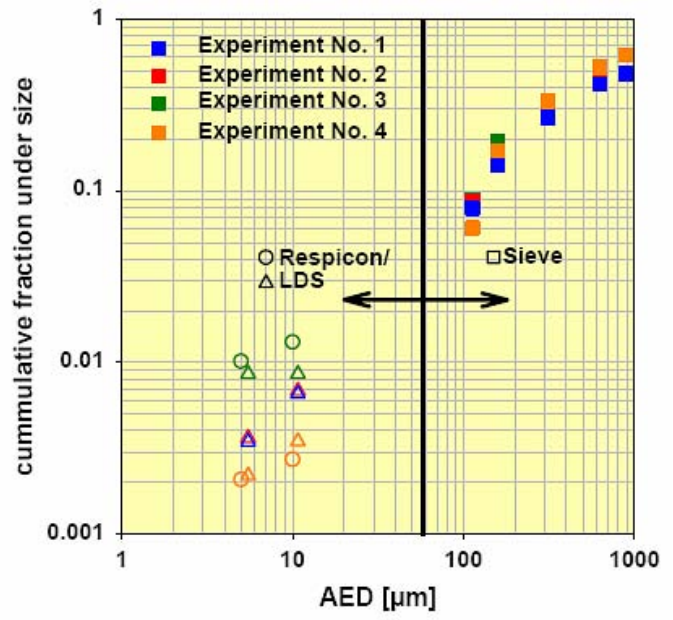

Figure 26. Phase 1 Glass Plate Test Cumulative Particle Size Distribution

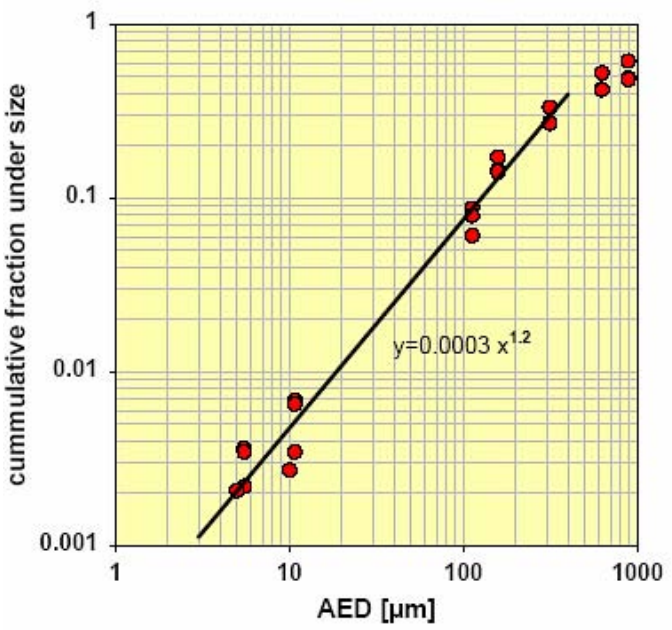

Figure 27. Phase 1 Glass Plate Test Cumulative Fraction Under Size

Fraunhofer Institut Toxikologie und Aerosolforschung

The combined particle size data from tests 1, 2, and 4 is shown as cumulative fraction vs. particle size, as shown in Figure 27. The size distribution fit to the data suggests a brittle material scaling law exponent of 1.2, close to 1. Due to the large scatter in the respirable particle size range, extrapolation from 10 to 100 µm AED is not possible; further particle size measurements in this range would be desirable in the future.

Preliminary results and conclusions from these glass plate-CSC jet impact tests are as follows:

- Under the experimental conditions used, the fragmentation process of the glass plates is reproducible and gives fairly consistent results. However, uncertainties remain (to be addressed in future testing).

    - These experiments did not allow us to exactly discriminate between primary (CSC jet/ projectile impact related) and secondary (chamber wall impact related) fragmentation processes. The secondary processes, however, appear to be small.

    - The amount of fragmented material escaping the aerosol collection box through the CSC jet entrance and exit holes could not be quantified and characterized.

- An aerosol collection chamber with uncovered walls (i.e., no Styrofoam sheets) can be used in the future. Collection chamber dimensions in the CSC jet direction should be of the order of 30 cm (12 inch). It would be desirable to close the CSC jet entrance and exit holes as soon as possible after CSC detonation. (NOTE: these suggestions were incorporated in subsequent Phase 2 surrogate testing [Molecke et al., 2004a]).

- The experimental set-up used in Phase 1 enables a suitable simulation of the CSC jet effect on the representative brittle glass material for the purposes of performing future comparison experiments with DUO_2 surrogate and spent fuel targets for the determination of the Spent Fuel Ratio as a function of aerosol particle size.

- The contribution of the explosive soot particles must be accounted for, primarily in the particles size range below 10 µm AED. (NOTE: chemical analysis of collected particles was initiated in the following Phase 2 test program [Molecke et al., 2004a]).

- The representative surrogate, leaded plate glass particle size distribution appears to follow universal power law behavior for brittle materials with, however, some uncertainties (observed scatter) in the respirable size range, < 10 µm AED. More detailed size and nuclide specific analyses in the respirable size range are required, and were implemented.

APPENDIX A

Supporting basic research on fragmentation of brittle material

W.Koch, Fraunhofer Institut für Toxikologie und Experimentelle Medizin, Germany, 2003

Objectives

The project on SFR is supported by complementary research conducted by the German project partners (GRS/FhG) in the laboratories of Fraunhofer ITEM (Institute of Toxicology and Experimental Medicine, Hannover, Germany) and Fraunhofer EMI (Ernst Mach Institute, Freiburg, Germany).

This research includes among others experiments with the Fraunhofer aerosol collection and classification unit which is described in detail in Mädler et al.1999. A series of experiments has been carried out to improve the understanding of the formation and release of airborne particles upon transient mechanical energy input into brittle material and to characterize its dependence on material properties and energy input. In context with the SFR program the specific aims are:

- studying the energy transfer between projectiles with various speeds (including a high speed projectile generated by a light gas canon and a shaped charge) and surrogate specimens with and without cladding;
- measuring the complete size distribution and check for existence of scaling laws for the size distribution found in previous research on fragmentation of brittle materials (Mädler and Koch, 1998, Nolte et al., 2002);
- correlating these results with preliminary tests obtained in experiments with shaped charge projectiles performed at SNL;
- deriving conclusions for the design for the aerosol collection and analysis device to be used in the ultimate spent fuel experiments.

Materials and methods

Aerosol collection and analysis system

A set-up shown in Fig. F1 was used for all experiments. It allows for complete in-situ characterization of the airborne release upon interaction of a brittle specimen with a small projectile. The apparatus consists of a vertical elutriation box separating the large debris from the airborne particles by suspending them in an upwards directed homogeneous airflow (flow velocity 25 cm/s which is equivalent to the settling velocity of particles with 100 µm AED). The air is entering a centrifugal classifier collecting particles in three size intervals covering the range between 100 and 21 µm. The fine fraction is further classified by conventional cascade impactors. The measured aerosol size range extends over three orders of magnitude from 0.1 to 100 µm AED. In addition, non-airborne fragments collected from the bottom of the vertical elutriator can be analyzed by off-line methods such as sieving or laser diffraction spectrometry so that the complete fragment size distribution is characterized.

The performance of the apparatus was evaluated in the laboratory in extended calibration experiments using various test aerosols of known aerodynamic size distribution. One of the important features of the apparatus is its good reproducibility due to the fact that the released fraction is entirely sampled in-situ, which

rules out errors usually associated with sampling small aerosol volumes from spatially inhomogeneous aerosols and from sample preparation for off-line analysis.

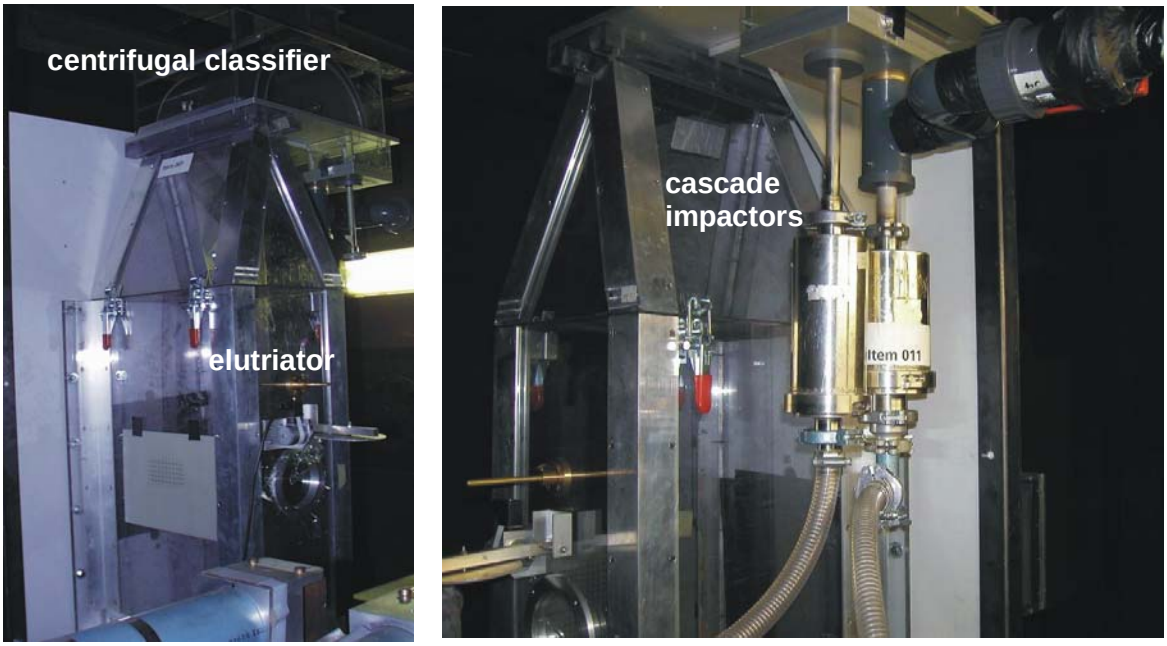

Fig. F1 Fraunhofer test rig for in-situ characterization of the airborne release.

The quantities of primary interest in the SFR program are:

- the cumulative airborne mass as a function of the aerodynamic diameter, $m_{airborne}(x_{ae})$;
- the cumulative airborne mass fraction as a function of the aerodynamic diameter, $Q_3(x_{ae})$.
- the release fraction smaller 100 μm AED, η_{100}, defined as $Q_3(x_{ae}=100\mu m)$;

Generation of transient mechanical energy load

The fragment analysis rig can be combined with various modes of transient energy transfer into a test specimen:

1. The test specimen is accelerated in a pneumatic gun and impacted horizontally against a hard target. The impact speed of small pellets can be as high as 200 m/s. Objects of 1 kg mass can be accelerated up to 100 m/s.

2. The test specimen is suspended inside the aerosol collection chamber and is hit by projectiles such as low speed rifle bullets (up to 1000 m/s), high speed light gas cannon projectiles (up to 3000 m/s) and shaped charge jets (up to 7000 m/s). The aerosol classification apparatus has been shown to securely sustain the pressure conditions associated with the operation of a shaped charge of xx g.

In all impact modes the test rig is sealed immediately after the collision process so that a complete mass balance of the fragmented specimen is achieved.

The pneumatic gun and rifle bullet test stand are established at the Fraunhofer ITEM. Test using the light gas cannon and shaped charges are performed at the Fraunhofer EMI (Fig. F2).

Fig. F2 Light gas cannon operated at EMI.

Summary of the main results

Impact experiments with small test pellets at low interaction speeds

A large number of experiments were performed using the pneumatic acceleration device and impacting unclad test pellets against a hard target. For these experiments the energy input, E, into the pellets is exactly known since it is simply given by

$$E = \frac{1}{2} m v^2 \qquad \text{F1}$$

where v is the measured impact velocity and m is the mass of the test specimen. Variation of the impact velocity between 13 and 200 m/s resulted in a wide span of W_m between 80 and 20000 J/kg. The well defined experimental boundary conditions and the good reproducibility of the experimental procedure allowed for a systematic study to find out the relevant parameters controlling the formation of the airborne fraction.

The experiments revealed a pronounced universality in view of the material properties and the size distribution of the airborne fragments. The data in Fig. F3 show a linear relationship between the release fraction, η_{100}, and specific energy input $W_m = E / m$. The variation of the slopes obtained from regression analysis for material specific experiments is less than a factor of two for the materials tested (see Table F1).

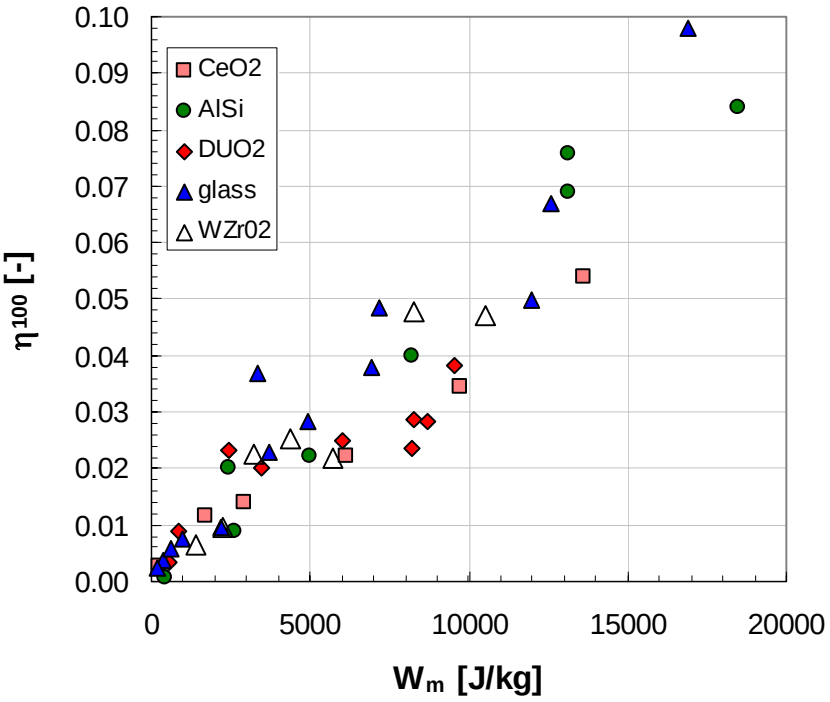

Fig. F3 Release factor obtained for impact experiments with small cylindrical pellets (1 cm diameter, 1 cm height)

We also found a universal power law function

$$Q_3(x_{ae}) = a(x_{aed})^{\nu} \qquad \text{F2}$$

describing the cumulative mass distribution of the airborne fragments as shown for a few examples in Fig. F4. The exponent ν takes values very close to one, irrespective of the material and the specific energy input. Thus the measurement of one point of the mass distribution allows for the prediction of the entire mass size distribution in the size range between 1 and 100 µm AED. In the submicron size range the scatter becomes quite large for some ceramic materials (DUO_2, AlSi) due to the fact that intra-grain boundary cracks are required for the formation of particles in this size range. From these results one can argue that for comparable modes of energy input, the spent fuel pellets being also brittle ceramic material behave very similar to the DUO_2, i.e., the SFR for the mass (< 100 µm, respectively < 10 µm) being very close to 1.

Table F1. Regression Parameter for the Data Points of Fig. F2

Material	slope [kg/J]	ρ [g/cm³]
AlSi	4.93E-06	1.6
CeO_2	3.64E-06	6.8
DUO_2	2.60E-06[1]	11
Glass	5.15E-06	2.2
WZrO	4.69E-06	10.3

[[1] The DUO2-value is somewhat lower. This is due to the data points belonging to impact energies above 5000 J/kg. Here, a significant quantity of the fragmented pellet material was sticking at the wall due to increased powder cohesiveness caused by oxidation of UO2 to U3O8.]

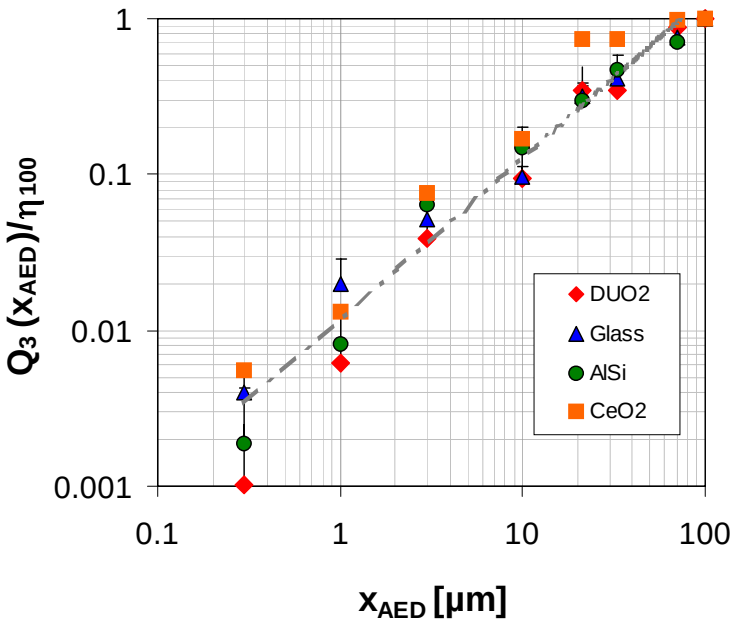

Fig. F4 Cumulative mass size distribution in the relevant size range normalized to its value at x_{AED}=100 µm: low speed pellet impact test.

However, a HEDD impact represents a hypervelocity impact with interaction speeds of the order of or larger than the speed of sound in the brittle material. Nothing is known about the size distribution of airborne fragments for these types of interactions. It would be highly speculative to extrapolate the above results, especially the size distribution law to the situations of a HEDD impact.

In addition, for HEDD interaction high local material temperatures are to be expected leading to the enrichment of volatile fission products in the small particle size range (< 10 μm). These volatile nuclides are specific for the type of spent fuel considered. Thus mass and nuclide distribution must be measured in all size fractions below 10 μm in each experiment of the envisaged aerosol test program for spent fuel.

In order to get information on the relationship between impact time and the formation of airborne particles a series of experiments with projectiles of various speeds impacting on test specimen suspended inside the vertical elutriation chamber was performed.

Impact experiments with rifle bullets on glass plates

Bullet impact experiments were carried out with a 7.2 mm projectile (lead with hard metal mantle) at impact velocities between 330 and 975 m/s. The different speeds were obtained by using different amounts of explosive powder in the ammunition. The projectile was impacted against glass plates of various dimensions. The aerodynamic size distribution of the airborne fragments again follows a power law (Fig. F5). However, a dependence of the exponent on the parameters such as impact speed or thickness of the plate cannot be completely ruled out. The exponent corresponding to the data points at high impact speed (black spheres) seems to be smaller than the exponent characterizing the trend of the data points at low impact speed (for example the green squares). In any case there is no distinct structure in the size distribution in the range between 10 and 100 μm, so that a linear interpolation between these two data points (on a log-log scale) describes the distribution function sufficiently accurate. Since this size range is exactly the one covered by the coarse particle classifier it would be possible to omit it in a future set-up for the spent fuel experiments. This would result in a considerable experimental simplification without loss of information.

The parameterization of the total amount of airborne material generated upon interactions of the glass plates with the projectile is more complicated compared to the pellet impact experiments. Whereas for pellet impact against a wall the specific energy input is known, this is not the case for the bullet impact. Particularly for thin targets a significant fraction of the bullet energy remains as kinetic energy with the bullet after it passed through the target. This is shown in Fig. F6, where the release fraction is plotted against the kinetic energy of the bullet before impact. Glass plates 30 by 30 mm with 22 and 5 mm thickness were impacted with a projectile (mass 7.2 g) at various velocities. The data for the 22 mm plate seem to be very well represented by a straight line, reflecting the same trend as obtained for the impacting glass pellet (See Fig. F2). If the total bullet energy were transferred into the plate the specific energy input calculated for the 3200 J impact on the 22mm-plate is W_m=60,385 J/kg. According to Table F1 the release fraction for this value of the specific energy input is $\eta_{100} = 5.15 \times 10^{-6} \times 60385 = 0.33$ which is roughly a factor of 2.5 higher than the value of 0.13 that was actually measured. This means that only 40% of the bullet energy is transferred into the 22 mm glass plate. This transfer efficiency seems to scale with the inverse of the plate thickness, at least for bullet energies smaller than 1600 J since, in this range the release fraction is approximately the same for the 5 mm and the 22 mm plates for the same bullet energy.

The release data obtained by variation of the lateral dimensions of the glass plates suggest that only a restricted area around the impact zone contributes mainly to the fine particle release. In Fig. F7 the measured values of release fraction are scaled with the ratio of the actual plate cross sectional area to the cross sectional area of the smallest one used in this series of experiments (i.e.A_0 = 30x30 mm²). The data seem to collapse into one single curve. Note that the scaling factor is 9 for the largest plates and the measured release fractions were actually a factor of 9 lower for the 90x90 plates as compared to the 30x30 plates. These findings could be helpful for the interpretation of results of future experiments with plate-like spent fuel specimen from research reactors, as envisaged to be performed in Phase 4 of the SFR program.

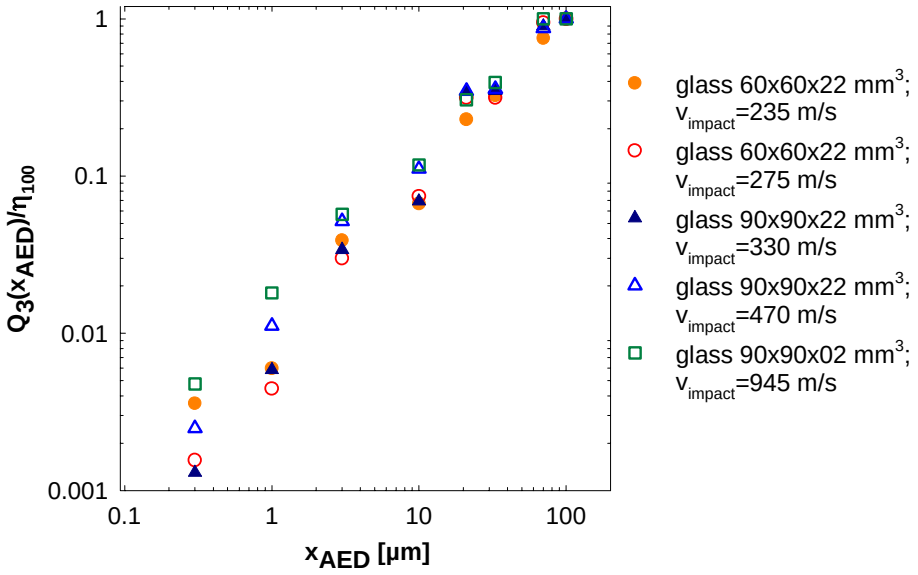

Fig. F5 Cumulative mass size distribution in the relevant size range normalized to its value at x_{aed}=100 µm: medium to high speed bullet impact test.

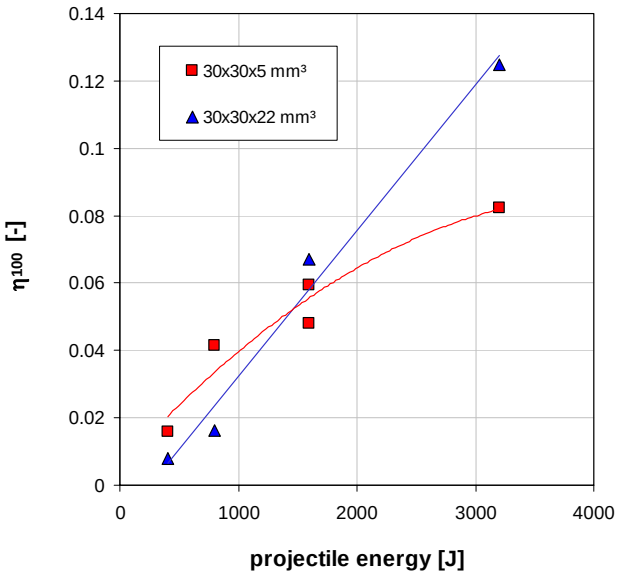

Fig. F6 Release fraction upon fragmentation by bullets impacting against glass plates.

The impact energy of 400, 800, 1600 and 3200 J correspond to impact velocities of 334, 473, 669, and 945 m/s.

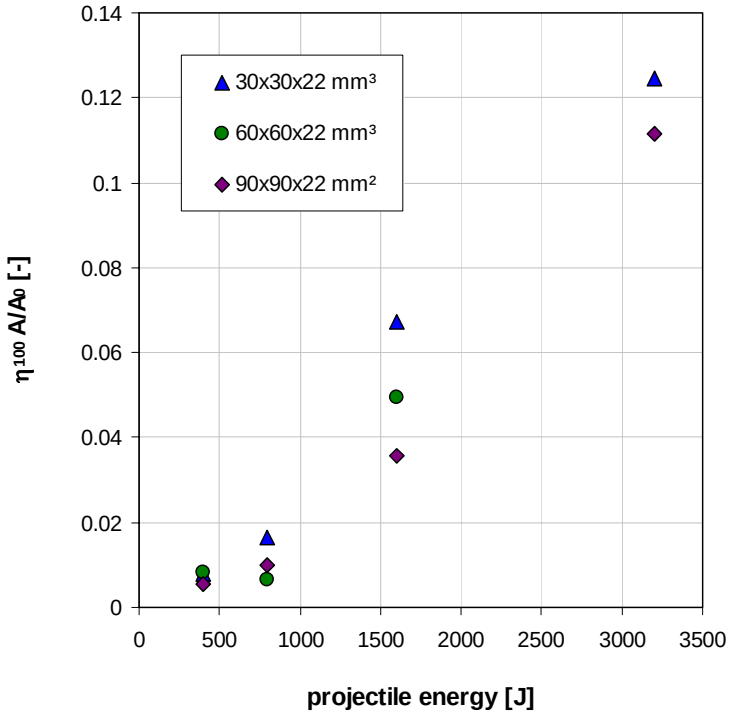

Fig. F7 Release fraction upon fragmentation when bullets impact against glass plates of different lateral dimension but the same thickness.

Impact experiments with bullets generated by a light gas canon

In order to check the above results for impacts of speeds above 1000 m/s similar experiments were performed using a light gas cannon operated by the Fraunhofer Ernst-Mach Institute, Freiburg, Germany. Steel spheres (diameter 4mm, mass 0.26 g) were impacted at a fixed speed of 2.9 km/s on 100x100 mm float and lead glass plates. The corresponding bullet energy is 1100 J.

The size distribution of the airborne fragments was measured using the Fraunhofer in-situ classification apparatus. The larger fragments were collected from the bottom of the chamber and were analyzed by sieving. In this way complete recovery of the mass of the glass plates could be achieved in the experiments. The size distribution law again follows a power function (Fig. F9) in the size range < 100 μm, however with significantly different slopes for the float glass plates and lead glass plate. In the size range below 100 μm the exponent ν takes values between 0.68 and 0.77 for the float glass plates whereas it 1.15 for the lead glass. The reason for this may be related to the different sound speeds in the two materials. This needs to be explored by further investigation.

The impact speed has obviously no influence on the general functional form of the size distribution. Interpolation between two data points (< 100 μm AED) on a log-log scale describes the cumulative size distribution in between these two points with sufficient accuracy.

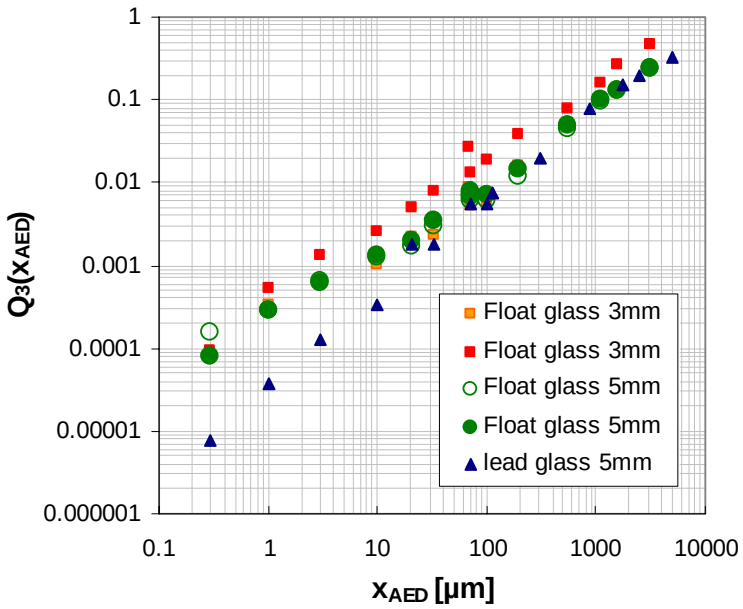

Fig. F8 Fragment size distribution obtained for the high velocity impact with glass plates.

Data above 100 µm obtained off-line by sieve analysis, airborne fraction characterized in-situ.

In experiment 2 (full red squares) the fragmentation seems to have been considerably more intense resulting in a η_{100}-value of 2% whereas in all other experiments 0.5% of the total mass of the glass could be attributed to particles with an aerodynamic diameter smaller than 100 µm. The latter value, however, fits quite nicely to the rifle bullet data obtained for much lower speeds but comparable bullet energy. This is seen in Fig. F9 where the same scaling was applied to the high speed sphere experiments as for the rifle bullet data.

Impact experiments using shaped charge jets

The logical next step is to apply the same experimental set-up and particle analysis procedure to test specimen hit by a shaped charge jet. This has not yet been successfully carried out in the context of the SFR program due to stability problems of the aerosol collection chamber. The chamber was recently reinforced and used successfully with a conical shaped charge of xx g explosive. These experiments were conducted in Germany at Fraunhofer EMI and are part of a German project to investigate the interaction of HEDD jets with high activity waste (HAW) glass surrogate material. Several experiments with clad and unclad cylindrical glass rods were performed. Unfortunately, size distribution data were not available at the time when this report was prepared.

As reported in the main text, preliminary CSC shots on lead glass plates and rod segments filled with CeO_2-pellets were carried out at SNL using a simplified non-ventilated aerosol collection chamber. A detailed experimental description and the results are presented in the main part of the report. In this Appendix, a comparison of experimental results obtained with the light gas cannon (LGC) projectile and the CSC jet for those experiments where sufficiently detailed information on the fragment size distribution is available is shown in Fig. F10. Relevant information on the corresponding experimental boundary conditions are summarized in Table F2.

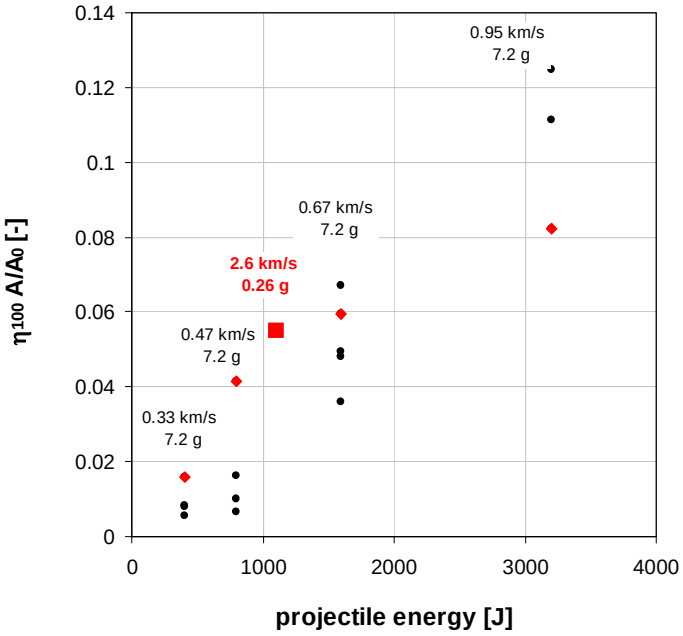

Fig. F9 Comparison of the scaled release fractions obtained for rifle bullet (small symbols) and high speed sphere impact experiments (big square).

Red symbols: 5 mm plate thickness; black symbols: 22 mm plate thickness.

Table F2. Experimental Parameters

Identification	Phase 1	Phase 2;3A and B	FhG EMI 0503
Projectile	HEDD-jet	HEDD-jet	Steel sphere
Impact velocity [m/s]	8000	8000	2900
Material of test specimen	Lead glass	CeO_2	Lead glass
Geometry	Thin plate (unclad)	cyl. rod segment	Thin plate (unclad)
Dimensions of fragmented specimen [mm]	50 x 50 x 5	9.2 x 32	100 x 100 x 5
Mass of fragmented material [g]	79.6	14.3	315.1

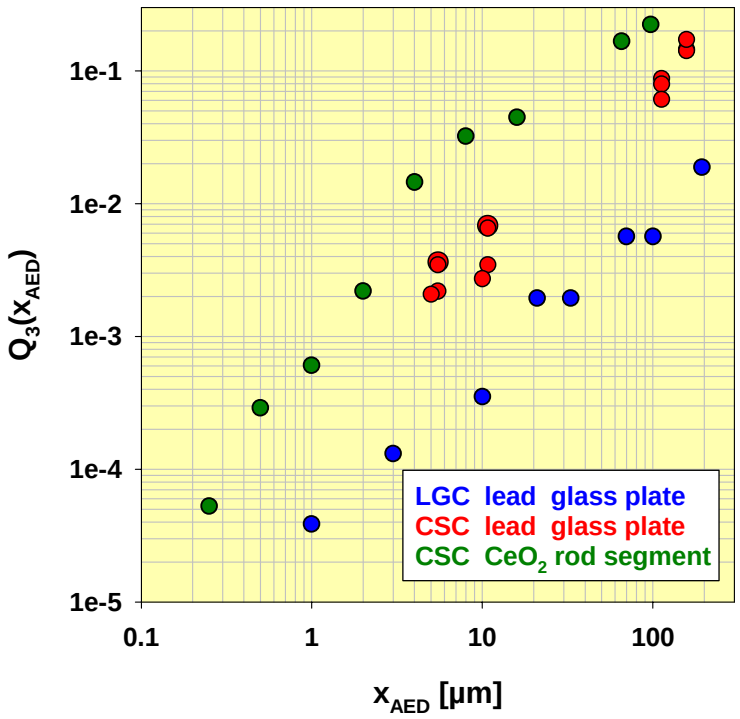

Fig. F10 Size distributions obtained for two different impact modes.

For the CSC experiments all fragments above 16 µm were analyzed by sieving. A full aerodynamic size distribution up to 100 µm is available only for the LGC-experiments.

A power law fit to the lead glass data results in an exponent of 1.2 for the CSC experiment and 1.15 for the LCG. The airborne fraction is approximately a factor of 10 higher for the CSC experiment with the 50x50 mm² plates as compared to the LGC interaction with the larger glass plates of 100 x 100 mm² . This could be explained by the scaling as applied to the data of Fig. F9 and/or higher impact energy of the HEDD jet which is however difficult to determine quantitatively.

The CeO_2-fragment distribution is somewhat steeper but still seems to be properly characterized by a power law function. In view of the spent fuel experiments this means that the aerosol size analysis can be performed in a simplified manner i.e. a detailed analysis in the small particle size range (< 10-20 µm) and the determination of the fragment mass distribution at 100 µm.

More meaningful conclusions on the interaction of a CSC jet with brittle material will be resulting form the current experiments at Fraunhofer EMI and ITEM as the final stage of a series of consistent experiments all performed with an identical aerosol analysis set-up delivering aerodynamic size data over the relevant size regime up to 100 µm AED. More such experiments should be carried out with geometrically the same test specimen of different brittle materials to improve the understanding of fine particle formation under the influence of hypervelocity impact and to check for a similar universality that was obtained for the release fraction in the pellet impact experiments.

The outcome of these systematic experiments could be a suitable surrogate material representing the spent fuel in view of the formation of airborne mass and the aerodynamic particle size distribution upon interaction with a hypervelocity jet. This would suggest further CSC impact tests using an array of fuel rod segments of surrogate material for example which would be more realistic for a fuel element. Correlating the fine particle formation with the macroscopic damage picture would provide a useful data base to estimate release data for other HEDD attack scenarios.

Conclusions

The following conclusions can be drawn from the supporting experiments:

- The functional form of the aerosol mass size distribution formed upon fragmentation of brittle material does not depend on the time scale of the transient energy input

- For the SFR tests involving spent fuel a simplified set-up can be used to measure the particle size distribution function. This should enable the measurement of the total airborne fraction and the mass and nuclide size distribution in the size range below 10 µm.

- Due to lack of sufficent and consistent experimental data a proper surrogate material for spent fuel exposed to hypervelocity interactions cannot yet be specified.

- Supporting experiments should be continued since they could provide useful data for extrapolation of the results of the SFR program.

References

Mädler and Koch, 1998; Mädler, L., Koch, W. Airborne Release of Fine Particles During Breakage of Brittle Materials. First Israel-German Bi-National Workshop on *Trends in Aerosol Research, Atmospheric and Industrial Aerosols*, Sheyfayim, Israel, 2.-3. 6. 1998

Mädler et al., 1999, Mädler, L., Koch, W., Lange, F., Husemann, K. (1999) In-Situ Aerodynamic Size Classification of Aerosols in the Size Range Between 0.1 and 100 µm for Dustiness Tests and Powder Characterization, Journal of Aerosol Science, 30: 451-465

Nolte et. al. 2002, Nolte, O., Lange, F.; Koch, W. Formation of fine particles in fragmentation of brittle material. 6. International Aerosol Conference, Taipei, Taiwan, 8.-13.9. 2002

APPENDIX B

Sandia National Laboratories

Operated for the U.S. Department of Energy by
Sandia Corporation
Albuquerque, New Mexico
87185-0783

date: December 11, 2003

to: Distribution

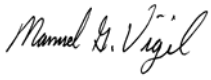

from: Manny Vigil, Dept. 2554, MS 1454, Consultant

subject:

Conical Shaped Charge Characterization and Performance Parameters (Abridged)

INTRODUCTION

The Explosive Technology Group (ETG) department personnel have been using the conical shaped charge "CSC1" for various applications or projects. I have had many discussions with ETG personnel wanting information on this shaped charge. Therefore, I thought it would be beneficial to all current and future ETG users of this shaped charge if I documented the information that we have obtained and developed on this shaped charge in recent years. This shaped charge is relatively expensive at a cost of about $730 each when at least 15 or more are purchased. Therefore, the information documented here should enable future users of this charge to conduct the minimum tests required to meet their objective. Looking at the number of these charges being ordered and tested, I believe that a lot of extra tests are being conducted before the desired timing for the jet arrival at the required location is empirically or experimentally obtained. The information documented here should allow future users of this charge CSC1 to precisely (within a microsecond) determine the jet tip arrival at the desired location and therefore, minimize the number of required tests.

These shaped charges were originally (a couple of years ago) purchased for use in the Determination of Dispersal Characteristics of Spent Nuclear Fuel and Other NRC-Licensed Material program, funded by NRC Project JCN W0397, B&R no. 311-15-315-397. This project required the smallest, precision conical shaped charge currently available and being produced in the USA. Very reproducible/repeatable jet parameters including alignment were required for this project. The jet must impact the center (+- 0.06 inches) of a 0.38 inch diameter spent fuel pellet at a standoff or distance of about 7.5 inches from the base of charge cone. The minimum explosive was desirable because some of these tests will be conducted in a hot cell in Area V. No other smaller, precision conical shaped charges could be located for this project.

This memorandum documents the characterization and performance parameters for the conical shaped charge, designated as CSC1 for this test program. The purchase price per charge was about $730. This is one of the smallest known precision CSCs. The xx gram explosive charge make it very suitable for many development and research projects.

EXPLOSIVE

This charge includes xx grams of PBX-N5 (95% HMX & 5% VITON A) explosive. The density is 1.7 g/cc. The detonation velocity is 0.84 cm/us. The Gurney velocity is 0.28 cm/us. The explosive exponent is 2.97.

LINER

The charge conical liner is copper (99% pure). The density is 8.96 g/cc. The bulk sound speed is 0.39 cm/us. The liner thickness is 0.029 inches. The weight is 21.6 grams.

HOUSING

The explosive housing is made of 6061-T6 aluminum. The housing has a tapered thickness.

PRECISION INITIATION COUPLER (PIC)

This includes a PIC assembly including a 0.xx gram of PBX-N5 explosive booster charge with a 1.7 g/cc density.

FLASH X-RAY RADIOGRAPHS

The flash X-ray radiographs for this charge are shown in Figures 5 through 9. The original 11 x 17 inch radiographs are in Department 2554 files. Some of the X-rays show curved jets etc. because on some of these tests the jet passed through a very small hole in a tungsten slug catching device before reaching X-ray head exposure station.

Table B2 lists the jet diameters. Table B3 lists the calculated jet tip velocities from X-ray radiograph measurements. The average jet tip velocity is about 0.83 cm/us.

PERFORMANCE PARAMETERS

The CSC1 shaped charge parameters are listed in Table B1.

SCAP CODE ANALYSES

SCAP code modeling/simulation of the CSC1 shaped charge graphical output was performed …

Figures A1 through A3 show the CSC1 geometrical configuration along with measured parameters used as input in the SCAP code modeling. The resultant SCAP geometrical model is shown in Figure A4. The jet formation, jet penetration into a steel target versus standoff, hole profile in steel, and other SCAP output graphical data are shown in the figures in Appendix A (*not included).*

CTH HYDROCODE ANALYSES

The CTH code predicted jet tip displacement versus time data are shown in Figure B10. This figure can be used to determine jet arrival time at a particular station. As shown in this figure, the calculated average jet tip velocity is 0.85 cm/us. The CTH code predicted slug displacement versus time data are shown in Figure B11. As shown in this figure, the calculated average slug velocity is 0.05 cm/us. The times in the above two figures are from the initiation of the Precision Initiation Coupler in the explosive. The 1.7 microsecond function time for the RP-2 detonator must be added to these times if the time relative to the firing set output is desired.

Professor Michael Huerta, University of Texas El Paso, UTEP, conducted all of the CTH hydrocode modeling/simulation work conducted for the CSC1 shaped charge. Three different CTH hydrocode runs for this shaped charge were performed. Output from three CTH code runs are available. The first two runs show the jet formation and propagation into air. The third run shows the jet propagation into air and then impacting a quartz plate.

SCAP CODE, CTH CODE, & FLASH X-RAY COMPARISONS

Table B4 includes the various shaped charge parameters compared for the following:

1. Flash X-ray measurements,
2. SCAP code predictions, and
3. CTH code predictions.

The code predicted and measured values in this table are in very good agreement.

FLASH X-RAY JET ARRIVAL TIMING FOR TESTING

During the flash X-ray testing for the characterization of the jet for this shaped charge CSC1, we discovered a very important timing issue. Initially, the jet arrival times were about 10 microseconds longer that the predicted SCAP and CTH code predictions. Since both codes predictions agreed, we decided to investigate the firing set system (Room 1305, John Lanoue and Adam Jimenez) function times. We discovered that this system has a function or through put time of about 9.7 microseconds. Therefore, you must add 9.7 microseconds to all predicted jet arrival times for any shaped charge involved in testing at this site.

For the CSC1 shaped charge the total times must include the following:

1. Room 1305 test site, firing set system function time: 9.7 us
2. RP-2 detonator function time: 1.7 us
3. PIC assembly function time: 2.0 us
4. Explosive detonation time and jet tip reaches base of conical liner: 10 us
5. Total time for jet to just be visible at base of copper conical liner: To = 23.4 us

The average measured jet tip velocity (Vj) per Table B4 is about 0.83 cm/us (0.327 in/us). This jet tip velocity remains constant until jet breakup which occurs at about 60 us. Therefore, you can predict the jet tip arrival time (Ta) as follows:

$$Ta = (Xj/Vj) + To = (Xj/0.327) + 23.4$$

Where,

Ta = Jet tip arrival at a distance Xj, (us = microseconds)
Xj = Desired distance or location for the jet tip from the base of the conical, copper liner (inches)
To = Time for the jet tip to reach the base of the conical liner or just be visible (23.4 microseconds)

CONCLUSION

This memorandum has documented the characterization and performance parameters for the CSC1 conical shaped charge. Flash X-ray radiographs were presented and these were used to measure several of the jet parameters including jet tip velocity, jet diameters, jet length, jet breakup time, jet alignment, slug velocity, slug diameters, etc.

SCAP code modeling/simulation predictions for the jet parameters in air were presented. SCAP code predictions for 20 different standoffs and for penetrating a steel target were presented. The SCAP code predictions for the jet parameters were compared to the CTH hydrocode predictions and also to the measured data from the Flash X-ray radiographs.

CTH hydrocode modeling/simulation predictions for the jet parameters in air were presented. The CTH code predictions for the jet parameters were compared to the SCAP code predictions and also to the measured data from the Flash X-ray radiographs. The agreement between the SCAP code, CTH code, and the measured data were very good.

Table B1. CSC1 Conical Shaped Charge Parameters

PARAMETER	VALUE
CSC LINER	
MATERIAL:	COPPER
WEIGHT	
EXPLOSIVE	
TYPE	PBX-N5 *
COMPOSITION	95% HMX, 5% VITON A **
WEIGHT	
DENSITY	1.7 g/cc
OUTSIDE DIAMETER	
LENGTH	
EXPLOSIVE HOUSING	
MATERIAL	ALUMINUM (6061-T6)
THICKNESS	TAPERED
OUTSIDE DIAMETER	
LENGTH	
PIC * ASSEMBLY**	
BOOSTER CHARGE	
TYPE EXPLOSIVE	PBX-N5
DENSITY	1.7 g/cc
EXPLOSIVE DIAMETERS	
WEIGHT	0.xx g
WAVE SHAPER	
MATERIAL	LEAD
WEIGHT	
TOTAL CHARGE EXPLOSIVE WEIGHT	
TOTAL CHARGE WEIGHT	
OPTIMUM STANDOFF (FOR MAX. PENET.)	7.1 in.
JET PARAMETERS	
TIP VELOCITY	0.79 cm/us ***
TIP DIAMETER	
AFT OF TIP DIAMETER	
LENGTH	7 in. ***
BREAKUP TIME	60 us ***
ALIGNMENT	
TAIL VELOCITY	0.2 cm/us ***
SLUG VELOCITY	0.1 cm/us ***
SLUG DIAMETER	0.08 in ***
SLUG LENGTH	2.0 in. ***
PENETRATION IN MILD STEEL	8.8 in. ***

[**Note**: multiple specific details have been removed from this table.]

* - HMX Formula: (4 Carbon, 8 Hydrogen, 8 Nitrogen, & 8 Oxygen atoms/molecules)

** - VITGON A: (60% Vinylidene Flouride, 40% Hexaflouropropylene Copolymer)

*** - PIC - Precision Initiation Coupler

Table B2. Test 15/ Measured Jet Diameters/ Radiographs

TEST DATE: 6/12/02

RADIOGRAPH	TIME (us)	Djt JET TIP DIA. (in.)	Djt JET TIP DIA. (mm)	Djtt JET TAIL OF TIP DIA. (in.)	Djtt JET TAIL OF TIP DIA. (mm)	Djat JET AFT OF TIP DIA (in.)	Djat JET AFT OF TIP DIA (mm)
1	55.592	0.18	4.6	0.18	4.6	0.05	1.27
2	60.552	0.18	4.6	0.18	4.6	0.05	1.27
3	65.397	NODATA	NODATA	NODATA	NODATA	NODATA	NODATA
4	70.710	0.20	5.1	0.13	3.3	0.04	1.0
5	75.498	0.20	5.1	0.13	3.3	0.04	1.0

Table B3. CSC1 Conical Shaped Charge Jet Tip Velocities/Flash X-Ray Diagnostic

TEST DATES: FEB. 4 - 15, 2002

TEST NO.	SO STANDOFF FROM .5"th.BLAST SHIELD (in.)	ΔX (in) (1)	ΔX (in) (2)	ΔX (mm)	Δt (us)	Vj JET TIP VEL. (mm/us)	Dj JET DIA. AFT. OF TIP (in.)
CSC1 -1	4						
T12			3.4	87.4	9.92	8.8	0.05
T23							
CSC1 -2	4						
T12			1.92	48.77	5.475	8.9	0.05
T23			1.86	47.24	5.562	8.5	0.05
CSC1 -3	4						
T12		2.302	1.634	41.51	4.934	8.4	0.07
T23		2.25	1.60	40.64	5.09	8.0	0.06
T3							0.05
CSC1 -4 (3)	4	ND	ND	ND	ND	ND	ND
CSC1 -5	7						
T34 (4)		1.415	0.99	25.16	4.98	8.3	0.06
CSC1 -6	7						
T13		4.69	3.283	83.4	10.01	8.3	0.05
CSC1 -7	0						
T13		4.464	3.125	79.375	9.96	8.0	
T45		6.742	4.719	119.87	15.297	7.8	
CSC1 -8	6	ND	ND	ND	ND	ND	ND

* - ACTUAL FILM MEASUREMENT ND - NO DATA

** - CORRECTED FOR FILM MAGNIFICATION

*** - HOLE IN TUNGSTEN TOO SMALL (0.10 "), LEADING HI VELOCITY PART OF JET CONSUMED, THEREFORE TIMES TOO EARLY(X-RAY)

**** - 0.5 " THICK LEXAN PLATE LOCATED 2.375 " AFT OF STEEL BLAST SHIELD, VELOCITY FROM SEPARATE FILMS, LEXAN CONSUMED SOME OF JET RESULTING IN LATE X-RAY TIMES

***** - NO X-RAY DATA, IMACON TIMES TOO EARLY, ONLY SAW DETONATION PRODUCT GASES JET

****** - SHORTENED TUNGSTEN FROM 2 TO 1.25 ", ONLY TEST WITH SHORTENED TUNGSTEN

Table B4. CSC1 CSC/CTH, SCAP Code, & X-Ray Measurements-Comparisons

PARAMETER	FLASH X-RAY MEASUREMENT	CTH CODE PREDICTION	SCAP CODE PREDICTION
JET TIP VELOCITY (cm/us)	0.8	0.8	0.83
SLUG VELOCITY (cm/us)	0.04	0.05	0.05
JET BREAKUP TIME (us)	59	40	NA
JET LENGTH (in.)/8.25”STANDOFF	8.5	7.9	7.7
JET DIAMETER/TIP (in)/8.25”	0.14	0.2 (t=20us)	0.1
JET DIAMETER/AFT TIP (in.)/8.25”	0.08	0.1	0.1
CONICAL LINER COL-LAPSE (us)	NA	20	20
H.E. DETONATION TIME (us)	NA	7.5	7.5
TIME/JET TIP AT 8.25 inches	49.3	39.5 **	39.0 ***

NA - NOT AVAILABLE
* - SOURCE: CTH/(6/22/02) RUN
** - TIME INCLUDES 2.0 us FUNCTION TIME FOR RP-1 DETONATOR
*** - TIME INCLUDES 2.0 us FUNCTION TIME FOR RP-1 DETONATOR PLUS 2.0 us FUNCTION TIME FOR PRECISION INITIATION COUPLER (PIC)

Figure B5. Flash X-Ray Radiograph of CSC1 Jet

(exposure times after firing set pulse: 45.5, 48.3, and 51.2 us)

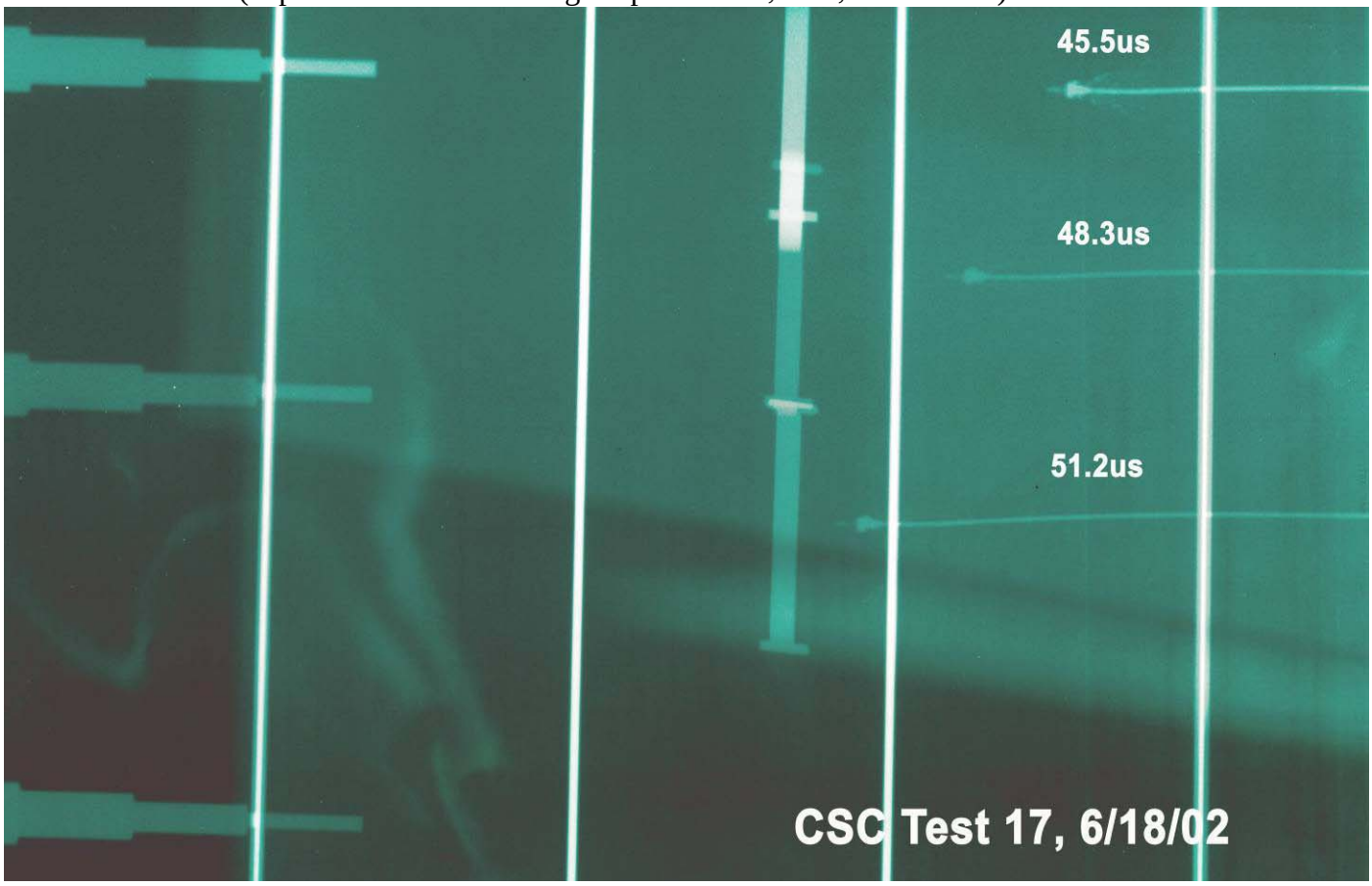

Figure B6. Flash X-Ray Radiograph of CSC1 Jet

(exposure times after firing set pulse: 66.26, 71.21 and 76.17 us)

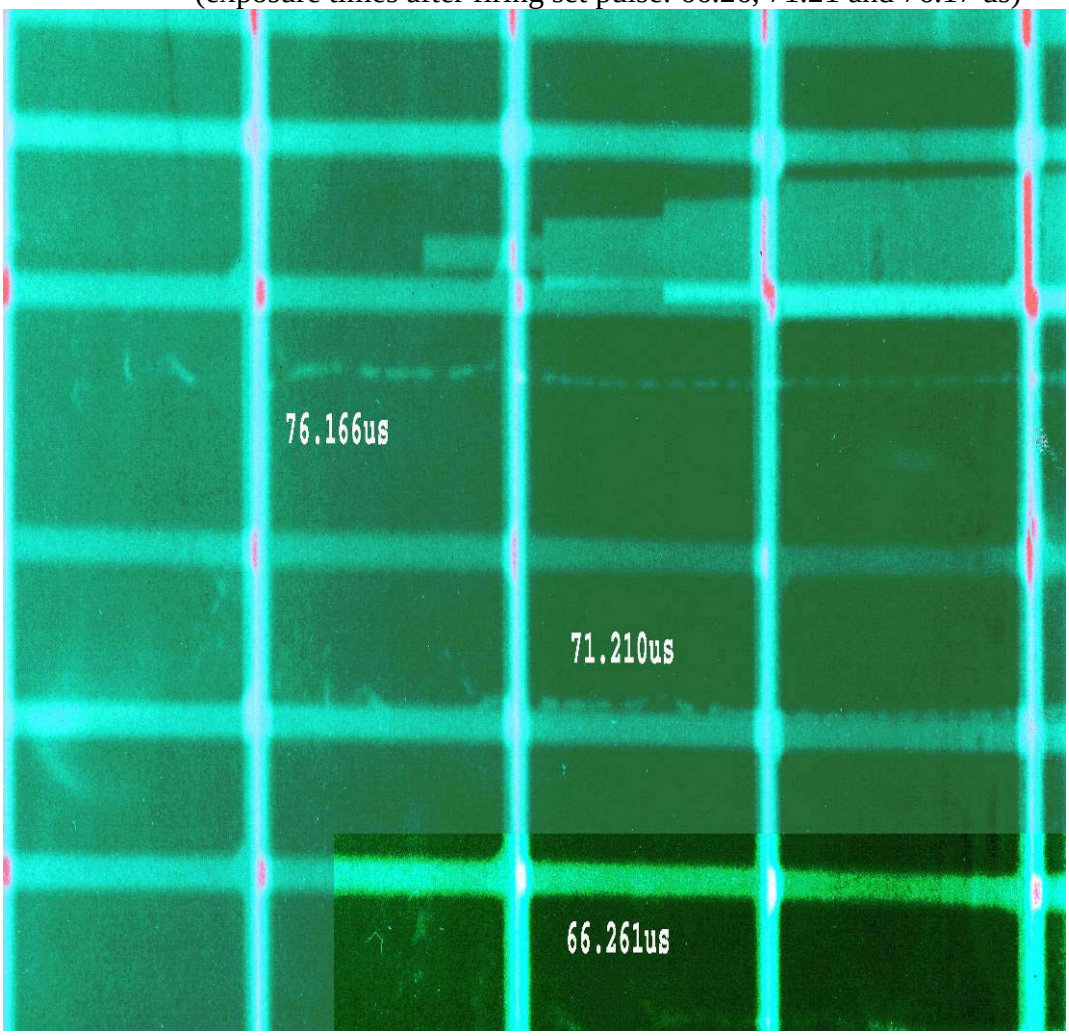

Figure B8. Flash X-Ray Radiograph of CSC1 Jet

(exposure times after firing set pulse: 70.69, 76.16 and 81.73 us)
Test II February 7, 2002

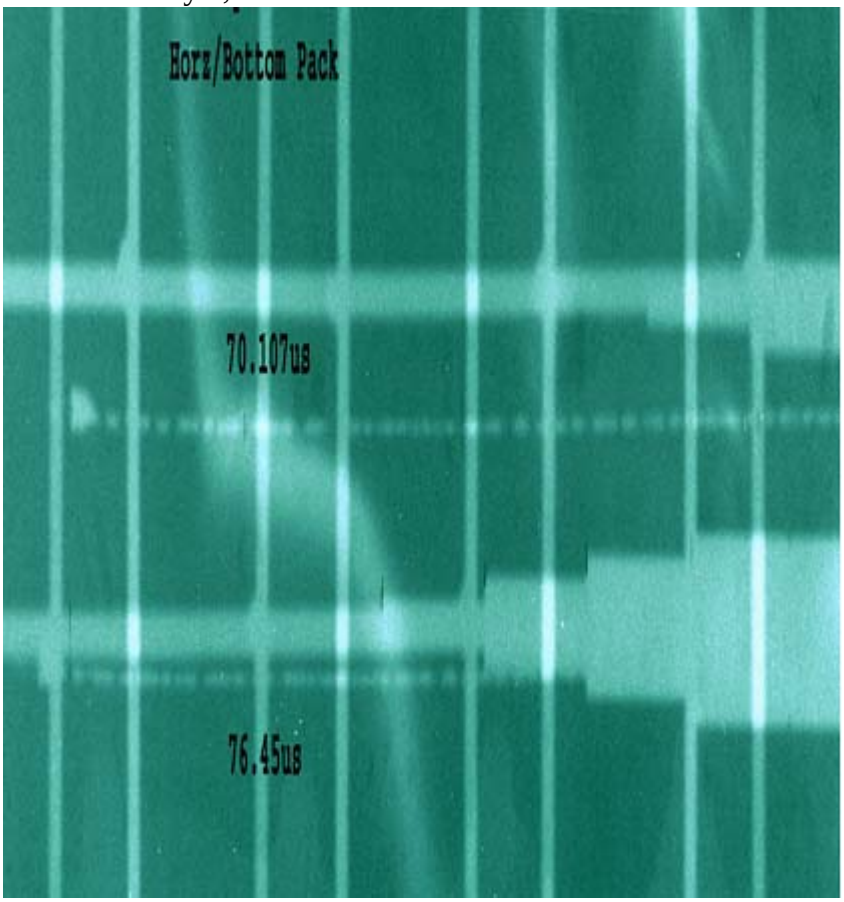

Figure B10. CTH Code Predicted Jet Tip Displacement Versus Time
CSC1 Conical Shaped Charge

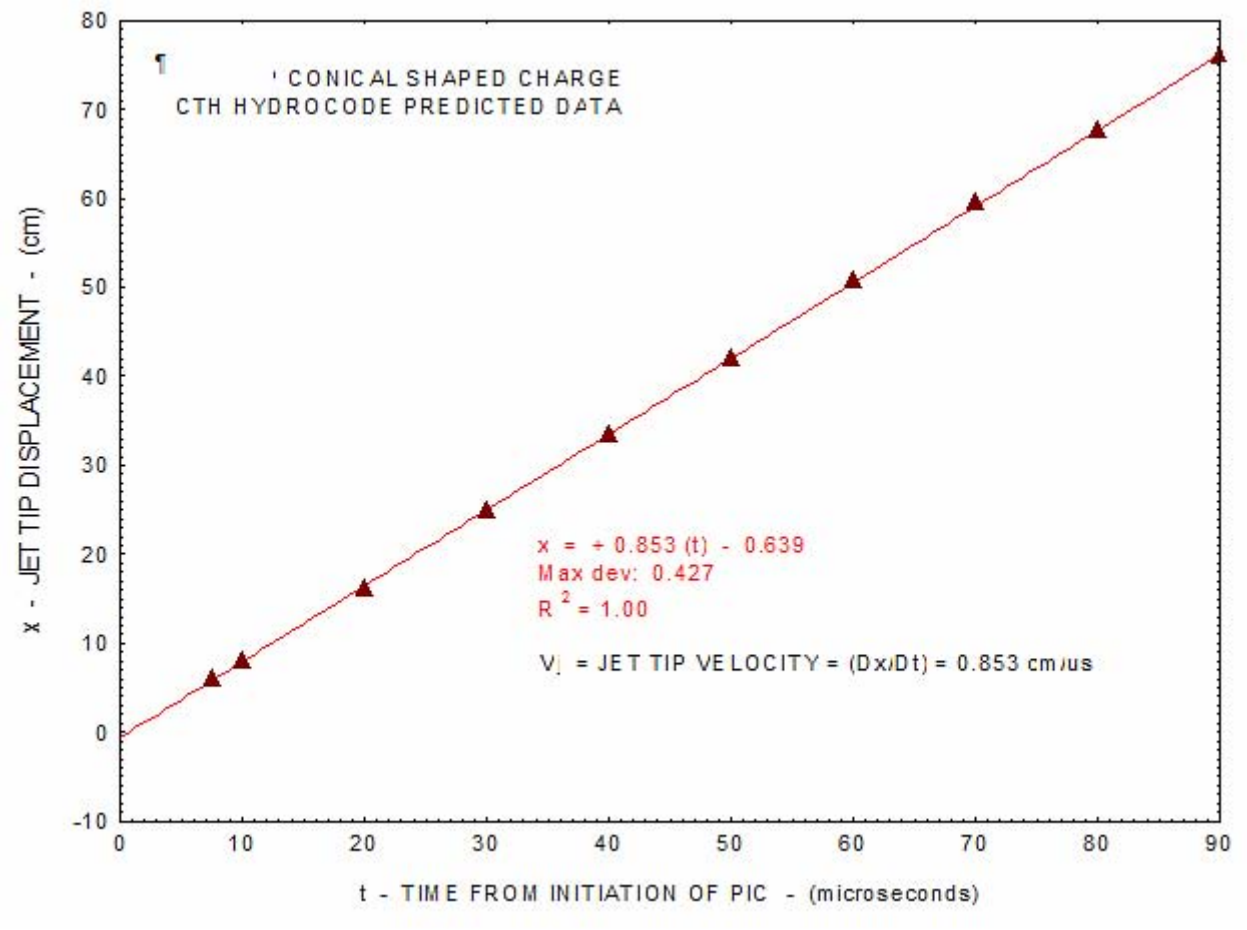

Figure B11. CTH Code Predicted Slug Displacement versus CSC1 Tip Conical Shaped Charge

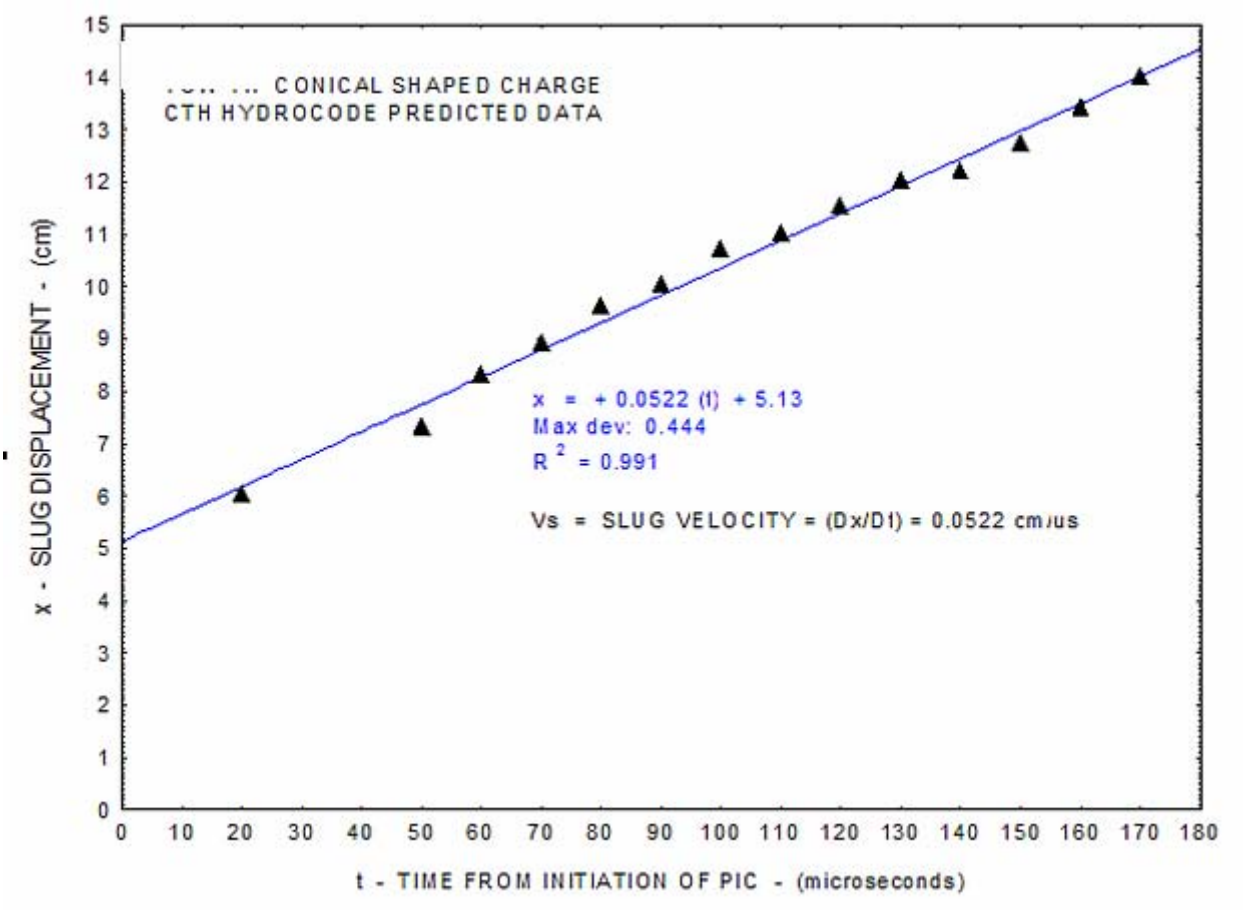

Copy To:

MS-0782	Marty Molecke, 6141
MS-0782	Richard Yoshimura, 6141
MS-1452	Michele Steyskal, 2552
MS-1454	Lloyd Bonzon, 2554
MS-1454	Adam Jimenez, 2554
MS-1454	Roy Dickey, 2554

APPENDIX C

Sandia National Laboratories
Operated for the U.S. Department of Energy by
Sandia Corporation
Albuquerque, New Mexico
87185-1454

date: August 28, 2003

to: Marty Molecke, MS-0718 (6141)

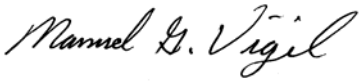

from: Manny Vigil, MS-1454 (2554), Consultant

subject:

CSC1 Conical Shaped Charge/Spent Fuel Pellet Test In Area-V Hot Cell/ Post Detonation Safety Concerns (Abridged)

INTRODUCTION

Per Marty Molecke's recent request, this memorandum documents information relative to the potential safety concerns after the detonation of a conical shaped charge (CSC), designated as "CSC1" in this test program, in a hot cell at the Area-V site. Information is included to address the following items:

1. Post-detonation reactant products from the detonation of the xx grams of PBXN-5 (LX-10) explosive in CSC1,
2. Potential for post-test, unsafe conditions, due to the initiation to detonation of undetonated explosive material, and
3. Information for technical justification and references.

EXPLOSIVE

The CSC1 contains PBXN-5 (also known as LX-10) explosive is composed of 95% HMX explosive and 5% Viton A binder (60% Vinylidene Flouride + 40% Hexafluoropropylene Copolymer). This explosive is a CHNO type explosive since it is mainly composed of carbon(C), hydrogen(H), nitrogen(N) , and oxygen(O) molecules. The chemical formula is:

Cx Hy Nw Oz = C(x) H(y) N(w) O(z) = C(1.4) H(2.7) N(2.6) O(2.6) = PBXN-5 explosive molecule

Where,
C(1.4) = 1.4 atoms of carbon
H(2.7) = 2.7 atoms of hydrogen
N(2.6) = 2.6 atoms of nitrogen
O(2.6) = 2.6 atoms of oxygen

REACTION PRODUCT HEIERACHY (References 1 and 2)

The simplest picture of how this reaction takes place is to visualize that in the zone where an explosive is detonating, the reactant molecule is completely broken down into its individual component atoms:

$C(x)\ H(y)\ N(w)\ O(z) > xC + yH + wN + zO$

These atoms then recombine to form the final products of the reaction. The typical products formed are:

$2N > N_2$
$C + O > CO$
$CO + O > CO_2$
$2H + O > H_2O$

Some explosives have more than enough oxygen to burn all of the carbon to CO_2. These explosives are therefore called over oxidized, or fuel lean. Some explosive compounds do not have enough oxygen to burn all the carbon to CO_2 and they are called under oxidized or fuel rich. The PBXN-5 explosive is 27% oxygen deficient, under oxidized, and fuel rich.

In all cases, the products formed can be estimated by using the following rule of thumb:

1. All of the nitrogen form N_2,
2. All of the hydrogen is burned to H_2O,
3. Any oxygen left after this burns carbon to CO,
4. Any oxygen left after this burns CO to CO_2, and
5. Any oxygen now let forms O_2 and traces of NOx (mixed oxides of nitrogen)

PBXN-5 (LX-10) EXPLOSIVE REACTANTS (Reference 3)

The overall reaction for under oxidized explosives is as follows:

$Cx\ Hy\ Nw\ Oz = 0.5y(H2O) + 0.5w(N2) + (0.5z - 0.25y)(CO2) + (x - 0.5z + 0.25y)(C)$

The overall reaction for PBXN-5 explosives is as follows:

$C(1.42)\ H(2.66)\ N(2.57)\ O(2.57)\ F(0.1) = 71.33(H2O)+1.29(N2)-0.04(CO2))+1.42(C) + F(0.17)$

In under oxidized reactions, some of the products themselves are fuels: specifically the free carbon, C, and the CO. After the detonation reaction is complete, the products may be free to expand into air. As they do so, they mix with the oxygen in the air and when the proper mixture with the air reached, they burst into flame and burn all the way to CO_2. This second reaction is called a fireball. Fireballs can also be fueled from other burnable materials, which have been mixed in with the explosive. Since very under oxidized explosives produce free carbon, which can form black, smoke and coat most surfaces in containment chambers, etc.

Therefore, clearly, from the above information and the fact that any remaining fuel after the detonation of the explosive is burned up in the fireball, there cannot be any fuel elements left in the residue.

CRITICAL TEMPERATURE FOR PBXN-5 EXPLOSIVE (Reference 4)

As an added technical justification, even if somehow there were some undetonated, post-test, particles of explosive. The only potential for initiation of the remaining explosive to detonation would be if the explosive were heated to above the critical temperature. Temperatures above this value can produce hot spots in the explosive to initiate a reaction in the explosive. For PBXN-5/HMX explosive, Figure C1 (Data taken from Reference 4) shows critical temperature versus explosive radius.

Per Figure 1, for explosive material with about 0.08 inch radius would require a critical temperature of about 496 degrees Fahrenheit. For explosive material about the size of the CSC1 explosive, the critical temperature required is about 384 degrees Fahrenheit to initiate the PBXN-5 explosive.

There is no foreseen mechanism by which the hot cell temperature would approach 384 to 496 degrees Fahrenheit to produce an unsafe explosive initiation condition post-test.

The information documented in this memorandum has addressed the items of concern listed in the introduction.

Please call me if you need additional information or have any questions about the information documented here.

MGV/2554/Consultant

Copy to:

MS-0718	Ken Sorenson	6141
MS-1454	Lloyd Bonzon	2554
MS-1454	Roy Dickey	2554
MS-1454	Michele Steyskal	2552
MS-1454	Manny Vigil	2554
MS-1454	Day File	2554
MS-	Ken Reil	6423
MS-	Sharon Walker	6400
MS-	Dick Coats	6400
MS-	Susan Longley	6400
MS-	Wade Goins	6400
MS-	Mike Gregson	6400
MS-	Others	6400

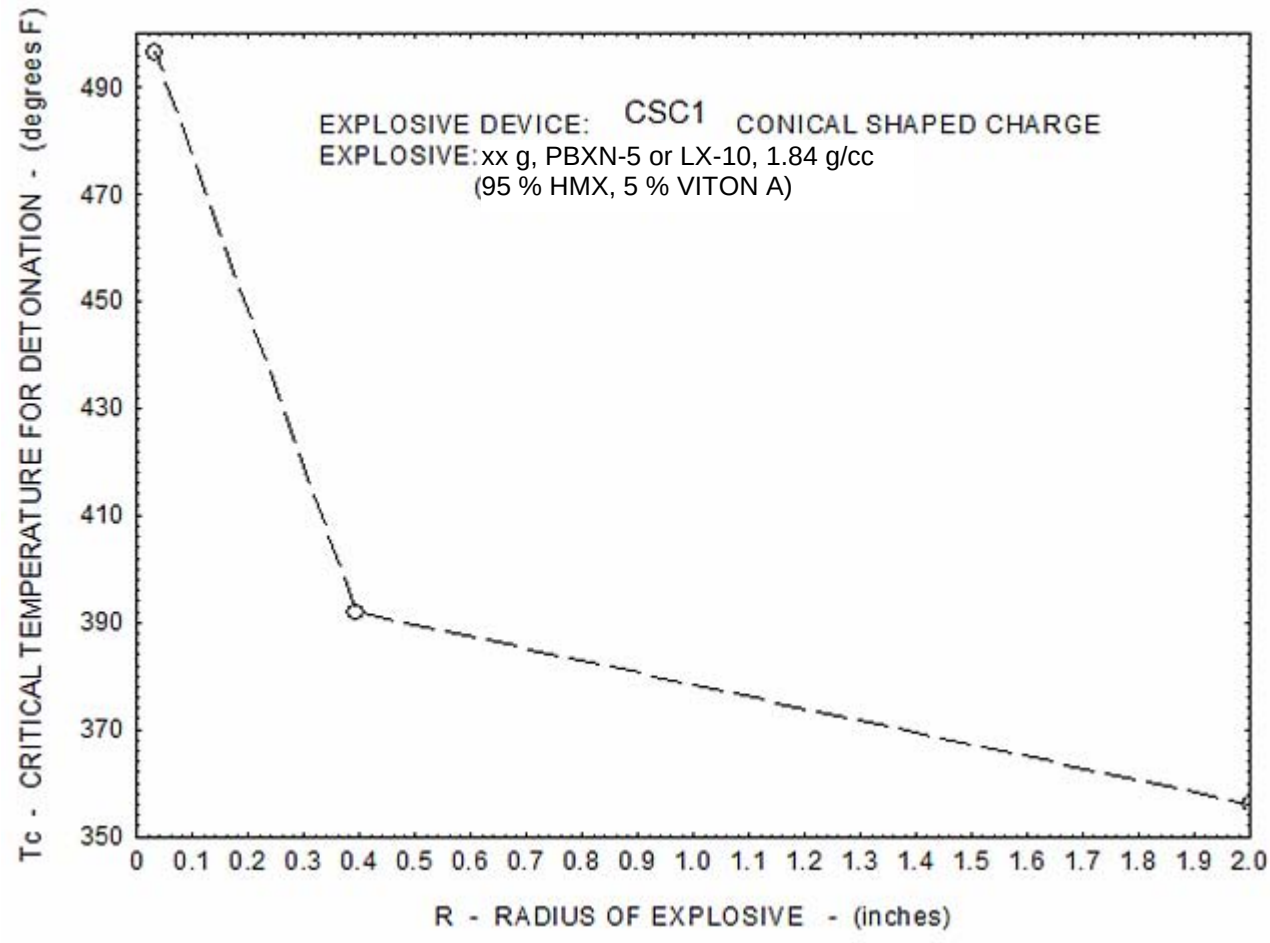

Figure C1. Critical Temperatures for the Detonation of PBXN-5 / LX-10 Versus Explosive Radius

REFERENCES:

1. P.W. Cooper, “Explosives Engineering”, Wiley-VCH, Inc., NY, NY,1996.

2. P.W. Cooper, S.R. Kurowski, “Introduction to the Technology of Explosives”, VCH Publications, Inc., NY, NY, 1996.

3. M.G. Vigil, “C-H-N-O Explosive Detonation Properties for Various Densities”, Sandia National Laboratories, Albuquerque, NM, SAND91-0603, June 1991.

4. J.A. Zukas, W.P. Walters, “Explosive Effects and Applications”, Springer, NY, NY, 1998.

REFERENCES

GRS/SNL, 2000. Gesellschaft für Anlagen- und Reaktorsicherheit and Sandia National Laboratories, "Joint GRS/SNL Proposal to Delineate the Ratio of Spent Fuel to Surrogate Aerosol Generation for More Accurate Prediction of Sabotage Consequences." Unpublished. July 2000.

Koch et al., 1999. Koch, W., W. Dunkhorst, and H. Lödding, *Design and Performance of a New Personal Aerosol Monitor,* Aerosol Sci. & Tech., Vol. (31), pg.231-246, 1999.

Koch et al., 2002. Koch, W., O. Nolte, and G. Pretzch, "Fragmentation of Brittle Material Under HED Impact – Results of Preliminary Experiments Performed at SNL in June 2002." Unpublished presentation, at the 4th Technical Meeting of International Working Group for Sabotage Concerns of Transport and Storage Casks, in Albuquerque, New Mexico, November 19-20, 2002. Fraunhofer Institut, Hannover, Germany, and Gesellschaft für Anlagen- und Reaktorsicherheit, Berlin, Germany.

Luna et al., 2002. Luna, R.E., H.R. Yoshimura, M.A. Molecke. DRAFT "Master Plan for International WGSTSC Experiments to Determine Spent Fuel Ratio/Fractionation for Spent Nuclear Fuel." Unpublished. September 2002.

Molecke et al., 2003. Molecke, M.A., H.R. Yoshimura, S.W. Longley, F. Lange, G. Pretzsch, W. Koch, O. Nolte, B. Autrusson, D. Brochard, N. Slater Thompson, and F.I. Young. Spent Fuel/Surrogate Aerosol Ratio Test Program and Preliminary Results, SAND2003-2706C. Presented at the 44th Annual Meeting, Institute of Nuclear Materials Management, July 13-17, 2003, Phoenix, AZ

Molecke et al., 2004a. Molecke, M.A., K.B. Sorenson, T.T. Borek, G. Pretzsch, F. Lange, W. Koch, O. Nolte, B. Autrusson, D. Brochard, N. Slater Thompson, R. Hibbs, and F.I. Young, Surrogate/Spent Fuel Sabotage: Aerosol Ratio Test Program and Phase 2 Test Results, SAND2004-1832. June 2004.

Molecke et al., 2004b. Molecke, M.A., M.W. Gregson, K.B. Sorenson, H. Tsai, M.C. Billone, Koch, O. Nolte, G. Pretzsch, F. Lange, W. B. Autrusson, O. Loiseau, N. Slater Thompson, R. Hibbs, F.I. Young, and T. Mo, Initiation of Depleted Uranium Oxide and Spent Fuel Testing for the Spent Fuel Sabotage Aerosol Ratio Program, SAND2004-4227J. Packaging, Transport, Storage and Security of Radioactive Material, Vol. 15(2), pp. 131-139 (2004). Ramtrans Publishing, UK.

Vigil, 2003a. Vigil, Manny. Internal memorandum to Distribution, "Conical Shaped Charge Characterization And Performance Parameters," December 11, 2003. Sandia National Laboratories, Albuquerque. (Abridged). [Appendix B]

Vigil, 2003b. Vigil, Manny. Internal memorandum to M.A. Molecke, "CSC1 Conical Shaped Charge/Spent Fuel Pellet Test In Area-V Hot Cell/Post Detonation Safety Concerns," August 28, 2003. Sandia National Laboratories, Albuquerque. (Abridged). [Appendix C].

DISTRIBUTION

U.S. Dept. of Energy, NNSA (4)
Office of International Safeguards
1000 Independence Ave., SW
Washington, DC 20585
Ronald C. Cherry, NA-243
Russell S. Hibbs, NA-243 (3)

U.S. Department of Energy, OCRWM
1000 Independence Ave., SW (6)
Washington, DC 20585
Nancy Slater Thompson, RW-30E (5)
J. Gary Lanthrum, RW-30E

U.S. Department of Energy, AL
Albuquerque Service Center (2)
P.O. Box 5400
Albuquerque, NM 87185-5400
A. K Kapoor
S. C. Hamp

U.S. Nuclear Regulatory Commission
Washington, DC 20555-0001 (10)
Branch Chief, RPERWMB, MS T-9F31
William R. Ott, MS T-9F31
Tin Mo, RES, MS T-9C34 (3)
F.I. Young, NSIR, MS T4-D8 (3)
Bernard H. White, SFPO, MS O13-D13
Robert E. Einziger, SFPO, MS O13-D13

Institut de Radioprotection et de Surete (5)
Nucleaire, IRSN/DSMR/SATE, BP17
92262 Fontenay-aux-Roses Cedex, France
Bruno Autrusson (4)
Olivier Loiseau

Gesellschaft für Anlagen- und (4)
Reaktorsicherheit (GRS) mbH
Kurfuerstendamm 200
10719 Berlin, Germany
Gunter Pretzsch (4)

Gesellschaft für Anlagen- und (4)
Reaktorsicherheit (GRS) mbH
Schwertnergasse 1
50667 Koln, Germany
Florentin Lange (2)
Wenzel Brücher (2)

Fraunhofer-Institut für Toxikologie und
Experimentelle Medizin, ITEM (5)
Nikolai-Fuchs-Str. 1
D-30625 Hannover, Germany
Wolfgang Koch (3)
Oliver Nolte (2)

Office for Civil Nuclear Security (3)
Department of Trade & Industry
146 Harwell
Didcot, OX11 0RA, UK
John M. Reynolds (2)
Bryan M. Reeves

Argonne National Laboratory (4)
Energy Technology Div., Bldg 212
9700 S. Cass Ave
Argonne, IL 60439-3838
Mike C. Billone (3)
Tatiana Burtseva

Robert E. Luna, Consultant (2)
10025 Barrinson NE
Albuquerque, NM 87111

Sandia Internal:

2552, MS 1452, M. Steyskal
2554, MS 1454 L.L. Bonzon
2554, MS 1454 R.R. Dickey
2554, MS 1454 M.G. Vigil
6140, MS 1089 F.B. Nimick
6141, MS 0718 D.R. Miller (4)
6141, MS 0718 M.A. Molecke (10)
6141, MS 0718 J. Sprung
6142, MS 0718 K.B. Sorenson (3)
6143, MS 0718 J. Danneels
6143, MS 0718 R.H. Yoshimura (5)
6143, MS 0718 R.F. Weiner
6782, MS 1143 D.T. Berry
6783, MS 1141 J.E. Dahl
6783, MS 1141 R.L. Coats
6783, MS 1141 M.W. Gregson (2)
6783, MS 1141 R.E. Naegeli
6784, MS 1146 K.O. Reil
6784, MS 1146 P.H. Helmick
6800, MS 0771 D.L. Berry
6860, MS 0736 M.C. Walck
9117, MS 0836 J.E. Brockman (2)
9117, MS 0836 D.A. Lucero
8945-1, MS 9018 Central Technical Files (1)
9616, MS 0899 Central Technical Library (2)

This page is intentionally blank.